iScience

CellPress
OPEN ACCESS

Article

Targeting CD36 determines nicotine derivative NNK-induced lung adenocarcinoma carcinogenesis

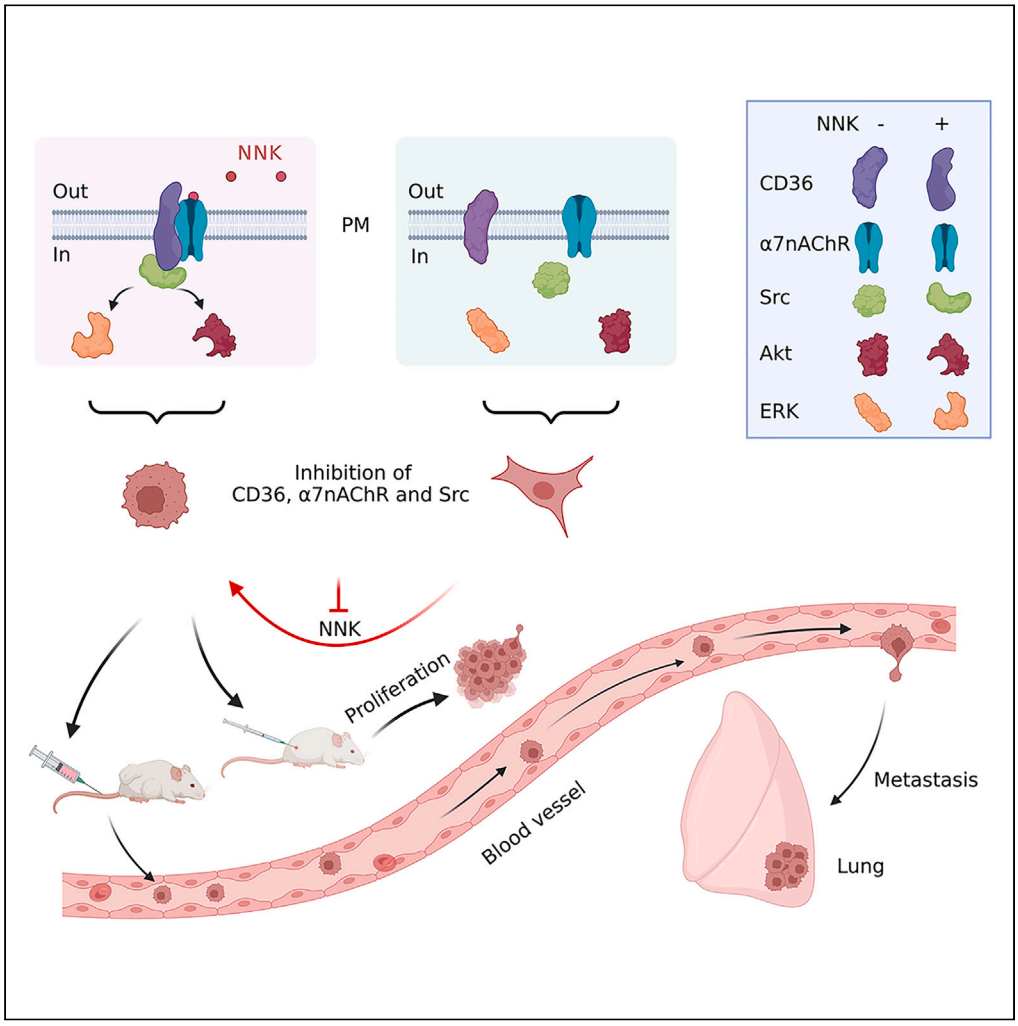

Ming-Yue Li, Menghuan Wang, Ming Dong, ..., Junbo Yi, George Gong Chen, Li-Zhong Liu

liulz@szu.edu.cn

Highlights

CD36 was overexpressed in smoking carcinogen-related LUAD tissues

CD36 interacted with α7nAChR and Src simultaneously upon NNK stimulation

CD36 located upstream and regulated the activity of Src/Akt/ERK1/2

CD36 inhibition counteracted NNK-induced LUAD carcinogenesis

Li et al., iScience 26, 107477
August 18, 2023
https://doi.org/10.1016/j.isci.2023.107477

iScience

CellPress
OPEN ACCESS

Article

Targeting CD36 determines nicotine derivative NNK-induced lung adenocarcinoma carcinogenesis

Ming-Yue Li,[1,2,4] Menghuan Wang,[1,4] Ming Dong,[1,2,4] Zangshu Wu,[1,2] Rui Zhang,[1,2] Bowen Wang,[1] Yuxi Huang,[1] Xiaoyang Zhang,[1] Jiaying Zhou,[1] Junbo Yi,[1] George Gong Chen,[3] and Li-Zhong Liu[1,5,*]

SUMMARY

Smoking carcinogen nicotine-derived nitrosamine ketone (NNK) is the most potent contributor to lung adenocarcinoma (LUAD) development, but the mechanism has not been fully elucidated. Here, we reported that fatty acid translocase CD36 was significantly overexpressed in both human LUAD tissues and NNK-induced A/J mice LUAD tumors. The overexpressed CD36 was positively correlated with Src kinase activation, smoking status, metastasis, and worse overall survival of patients with smoking history. Upon NNK binding with α7 nicotinic acetylcholine receptor (α7nAChR), sarcolemmal CD36 was increased and it interacted with surface α7nAChR and cytosol Src simultaneously, which in turn activated Src and downstream pro-carcinogenic kinase ERK1/2 and Akt, and finally caused LUAD cells to form subcutaneous and pulmonary metastatic tumors. This process could be blocked by CD36 knockdown and CD36 irreversible inhibitor SSO. Furthermore, the effect of NNK was inhibited obviously in CD36$^{-/-}$ A/J mice. Thus, targeting CD36 may provide a breakthrough therapy of LUAD.

INTRODUCTION

Lung cancer is the most frequent cancer and leading cause of cancer death worldwide.[1] And lung adenocarcinoma (LUAD) is the predominant subtype accounting for 40%–45% of all lung cancer cases with obvious rising incidence.[2] Although targeted therapy with such as epidermal growth factor receptor tyrosine kinase inhibitors shows preliminary clinical prospects, the treatment has been hindered by acquired resistance.[3] Therefore, there remains an urgent clinical need to identify new molecular targets for therapeutic interventions in lung cancer.

Since about 80% of lung cancers develop in current or former tobacco smokers, cigarette smoking outweighs all other risk factors.[4] Among the numerous carcinogenic agents in tobacco products, 4-methylnitrosamino-*l*-3-pyridyl-butanone, also known as nicotine-derived nitrosamine ketone (NNK), is a major contributor to lung carcinogenesis.[5] NNK could diffuse through the cell membrane and induce DNA adducts to activate mutations in proto-oncogenes and inactivate tumor suppressor genes. Furthermore, the signaling events induced by NNK through nicotinic acetylcholine receptors (nAChRs) contribute significantly to the oncogenic process.[6] Five subunits of nAChRs form homomeric or hetero-pentamer channels, which composed of either identical α subunits (α7 or α9) or combinations of α and β subunits (α2–α6, or α10 subunits together with β2–β4 subunits).[7] Several alpha (α1, α3–α7, α9, α10) and beta (β2 and β4) nAChR subunits have been identified in human airway epithelial cells and lung tumors.[8–10] Especially, the homomeric α7nAChR has been implicated as the primary receptor facilitating NNK-mediated cell proliferation through engaging various signal transduction molecules and transcription factors.[7] The full-spectrum molecular events in NNK inducing LUAD carcinogenesis through α7nAChR need to be deeply elucidated.

Fatty acid translocase CD36 (85-88KD) is a transmembrane glycoprotein with a relatively large extracellular domain. Both its amino and carboxyl termini are located within the cytoplasm.[11] CD36 has been identified as a key long-chain fatty acid receptor and transporter in the myocardium and skeletal muscle.[12] Fyn, one of Src family members, is associated with surface CD36 to form CD36-Fyn complex and regulate fatty acid PA (palmitic acid) uptake in skeletal muscle cells.[13,14] Some studies also suggest that CD36 is amplified and drives several kinds of carcinoma progression.[15–18] The non-receptor tyrosine kinases Src family include Src (also as c-Src), Fyn, Yes, Fgr, Yrk, Lyn, Hck, Lck, and Blk, which localize within the cytosol and transduce signals between cell surface proteins and other intracellular proteins, including transcription factors.[19]

[1]Department of Physiology, School of Basic Medical Sciences, Shenzhen University Medical School, Shenzhen University, Shenzhen 518055, Guangdong, China

[2]GuangZhou National Laboratory, No.9 XingDaoHuanBei Road, Guangzhou International Bio Island, Guangzhou 510005, Guangdong Province, China

[3]Department of Surgery, Faculty of Medicine, The Chinese University of Hong Kong, Hong Kong, China

[4]These authors contributed equally

[5]Lead contact

*Correspondence: liulz@szu.edu.cn

https://doi.org/10.1016/j.isci.2023.107477

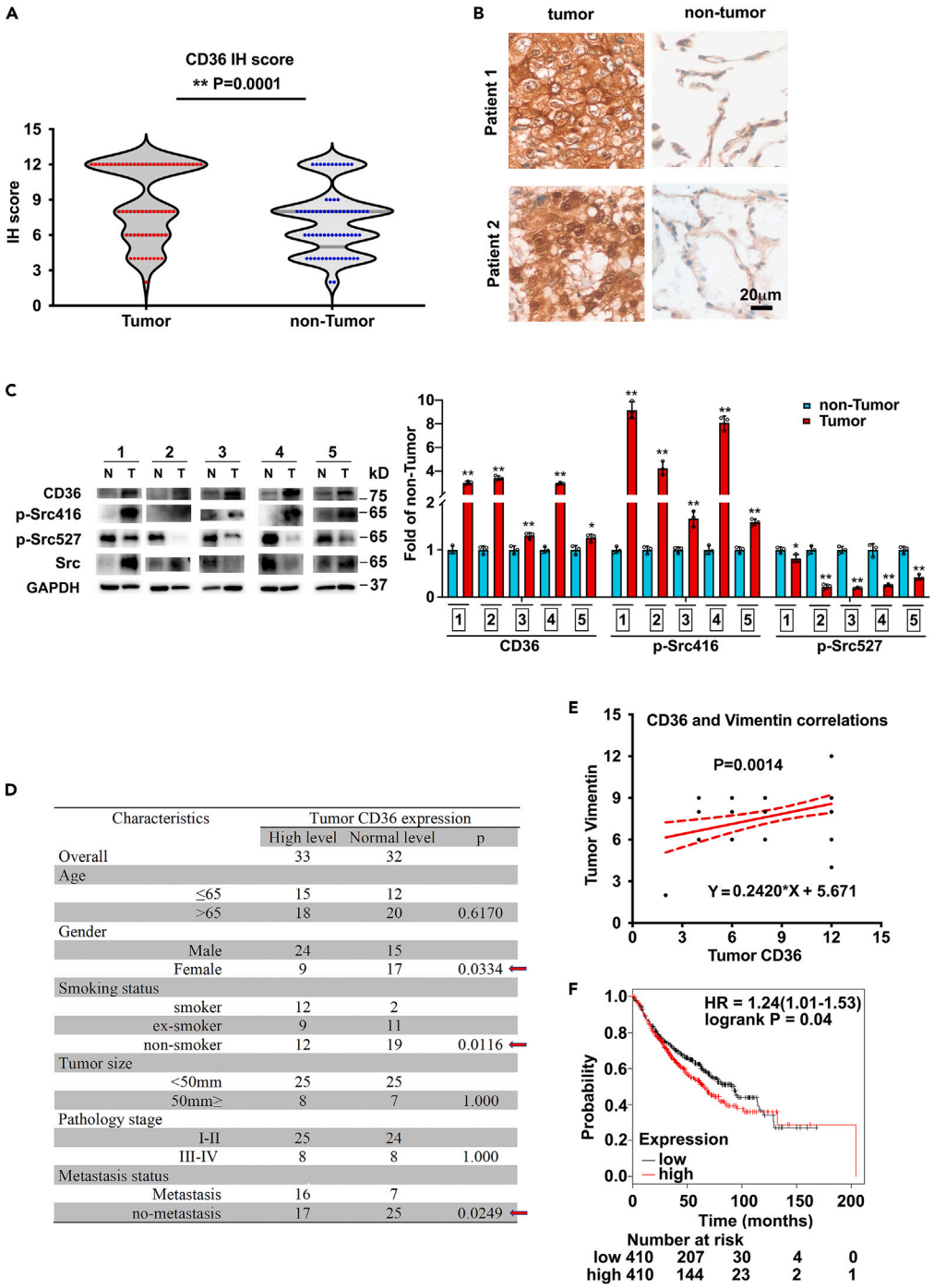

Characteristics	Tumor CD36 expression		
	High level	Normal level	p
Overall	33	32	
Age			
≤65	15	12	
>65	18	20	0.6170
Gender			
Male	24	15	
Female	9	17	0.0334
Smoking status			
smoker	12	2	
ex-smoker	9	11	
non-smoker	12	19	0.0116
Tumor size			
<50mm	25	25	
50mm≥	8	7	1.000
Pathology stage			
I-II	25	24	
III-IV	8	8	1.000
Metastasis status			
Metastasis	16	7	
no-metastasis	17	25	0.0249

Figure 1. The overall upregulated expression of CD36 and its positive correlation with smoking status and metastasis in human LUAD tissues

(A) The overall level of CD36 in LUAD tissues was upregulated relative to the paired adjacent normal tissues. The stained tissues were scored 1 to 12 according to the IRS method and expressed as Violin plot. Wilcoxon signed ranks test was used to compare the values between tumor tissues and non-tumor tissues (**$p < 0.01$).

(B) Representative immunohistochemical staining of CD36 expression in human LUAD tumor tissues. Lung tissue sections were stained with CD36 antibody and examined. Bar: 20 μm.

(C) Higher levels of CD36 were associated with higher activity of Src kinase in human LUAD tumor tissues. CD36, *p*-Src416, *p*-Src527, and Src protein levels were examined in 5 pairs of specimens. The relative intensity of protein bands was

Figure 1. *Continued*
summarized by column figure. The values indicate the mean ± SD of three independent experiments (N stands for non-tumor tissue, T stands for tumor tissue; *$p < 0.05$ and **$p < 0.01$ vs. N condition).
(D) Baseline demographic characteristics of 65 human LUAD patients underwent CD36 analysis. The clinic-pathologic features in patients with relative expressing CD36 were compared using Pearson's chi-squared test or Fisher's exact test for categorical variables. $p < 0.05$ was considered statistically significant.
(E) Positive correlation of CD36 and Vimentin in LUAD tumor. The correlation of CD36 and Vimentin expression levels in 65 LUAD tumor tissues was analyzed. A positive correlation between CD36 and Vimentin in lung tumor was shown ($p < 0.01$).
(F) Negative relationship between CD36 and survival probability on NSCLC patients with smoking history. The survival probability (overall survival) of the two groups of patients (n = 820) with high and low CD36 expression in NSCLC tissues was analyzed based on online survival analysis software: Kaplan-Meier plotter. High-level CD36 was significantly related to poor survival probability in NSCLC patients ($p < 0.05$).

Increased expression of Src and high levels of Src kinase activity, but not Fyn, have been reported in non-small-cell lung cancer (NSCLC), particularly in LUADs.[20] Src becomes activated in response to NNK and induce lung cancer cell migration and invasion.[21] Upon activation, Src phosphorylates multiple substrates including Akt and ERK, which is required for NSCLC, glioblastoma multiforme, and gallbladder adenocarcinoma cell proliferation/spreading.[20,22,23] The previously described findings indicate that CD36 might be involved in carcinogenesis of different tissues, including LUAD. However, upon NNK stimulation, there is no report on whether CD36 participates in NNK-induced carcinogenesis of LUAD. Here, we have revealed the pivotal role of CD36 in NNK-induced LUAD carcinogenesis via α7nAChR-CD36-Src signal axis, which is a potent therapeutic target for LUAD tumor.

RESULTS

CD36 expression was upregulated and positive correlation with smoking status and metastasis in human LUAD

To determine whether CD36 was overexpressed in LUAD and correlated with patient prognosis, immunohistochemistry (IHC) was performed in 65 cases of LUAD tissues (Table S1). Statistically, the CD36 overall expressions were upregulated significantly in LUAD cancer tissues than in normal adjacent tissues ($p < 0.001$, Figure 1A). The representative results of CD36 overexpression in LUAD were shown in Figure 1B. While phosphorylation at Tyr416 of Src kinase upregulates enzyme activity, phosphorylation at Tyr527 in Src carboxy-terminal tail renders the enzyme less active.[24] In 5 randomly selected paired LUAD specimens, the upregulated CD36 expression exhibited a positive correlation with Src activity (Figure 1C). Correlation analysis showed the high CD36 level was significantly associated with gender ($p = 0.034$), smoking status ($p = 0.0116$), and metastasis status ($p = 0.0249$) of LUAD patients (Figure 1D). It was worth noting that due to the limitation of our database, there were 14 smokers and 19 ex-smokers among male LUAD patients, while there were only 2 ex-smokers among female LUAD patient (others were non-smokers). This might cause bias to evaluate the relationship between smoking-related CD36 expression and gender here. It is still necessary to recruit more female patients in future studies. Nevertheless, CD36 expression correlated with smoking history positively. Further, the high expressions of CD36 and vimentin were positive-related in LUAD tumors ($p = 0.0014$) (Figure 1E). It was clearly known that vimentin was the well-characterized biomarker of metastasis during lung carcinogenesis.[25] Regarding NSCLC patients with smoking history, higher CD36 expression displayed a reduced overall survival-based online Kaplan-Meier plotter analysis (Figure 1F).

Increased expression and sarcolemmal distribution of CD36 were evidenced during NNK-induced A/J mice LUAD development

The tumors in A/J mice induced by NNK were pathologically confirmed to be adenocarcinomas.[26] IHC results showed that CD36 levels were significantly increased in lung tumor tissues compared to the normal lung tissues of A/J mice ($p < 0.0001$, Figure 2A and Table S2). The representative results showed that CD36 expression was upregulated in NNK-induced lung tumors at all time points between weeks 14 and 16 (Figure 2B). Consistently, CD36 expression and activity of Src, ERK, and Akt kinase were increased in the NNK-induced lung tumor tissues when compared with those of the control groups (Figure 2C). Next, CD36 sarcolemmal translocation during NNK-induced LUAD development was detected. Na^+/K^+ ATPase was used to label the cell membrane. Since the work results showed the Src activity increased in LUAD tumors (Figures 1C; 2C), and CD36 correlated with tumor metastasis positively (Figures 1 D and 1E), the increased sarcolemmal CD36 might initiate the metastasis of LUAD cells, which was similar as the report

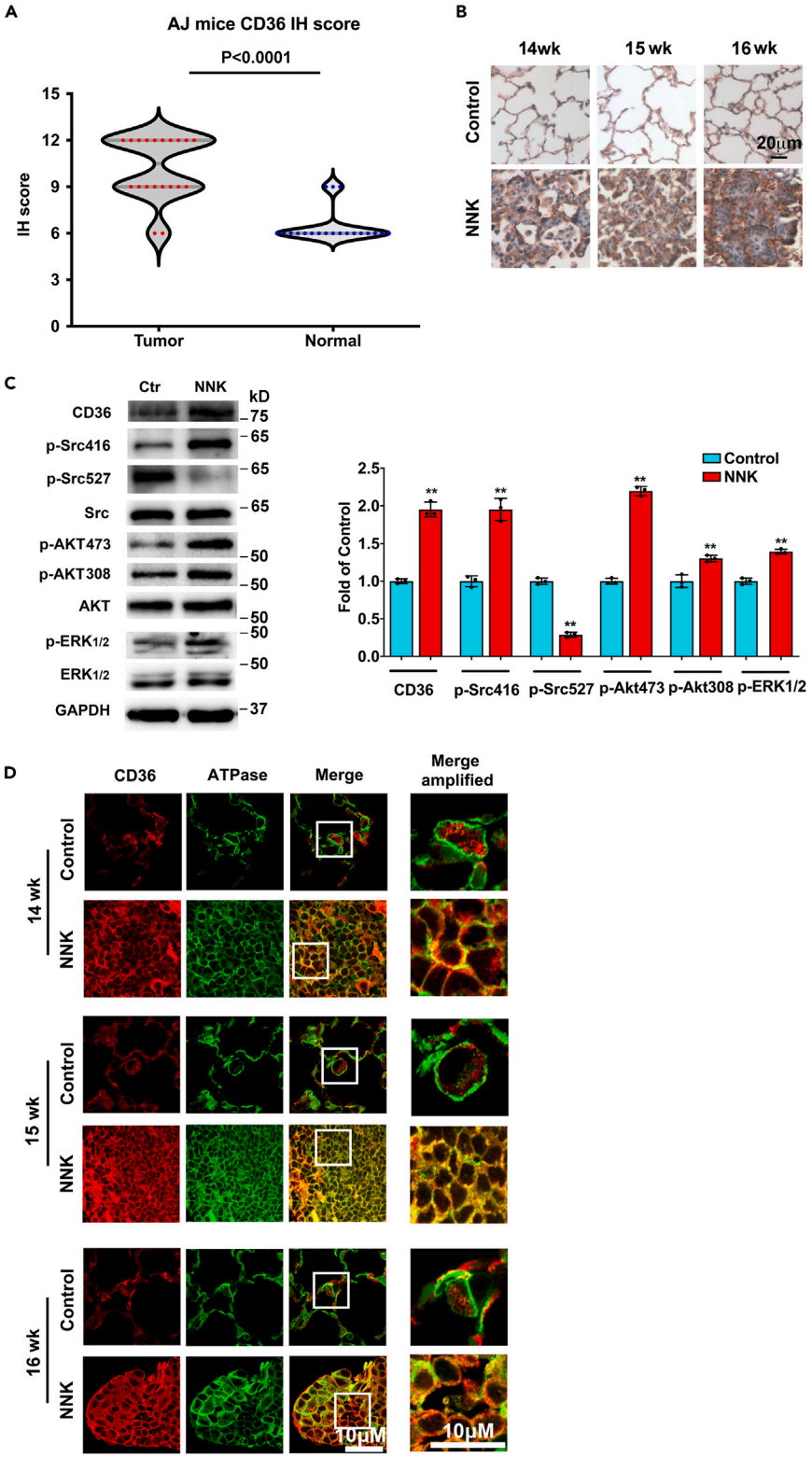
A
AJ mice CD36 IH score
P<0.0001
IH score
15
12
9
6
3
0
Tumor
Normal
B
14wk
15 wk
16 wk
Control
NNK
20μm
C
Ctr
NNK
kD
CD36
p-Src416
p-Src527
Src
p-AKT473
p-AKT308
AKT
p-ERK1/2
ERK1/2
GAPDH
75
65
65
65
50
50
50
50
50
37
Control
NNK
Fold of Control
2.5
2.0
1.5
1.0
0.5
0.0
CD36
p-Src416
p-Src527
p-Akt473
p-Akt308
p-ERK1/2
D
CD36
ATPase
Merge
Merge amplified
14 wk
15 wk
16 wk
Control
NNK
10μM
10μM

Figure 2. CD36 overexpression and its sarcolemmal translocation during NNK-induced A/J mice LUAD development

(A) The levels of CD36 in A/J mice LUAD tissues and normal tissues. The stained tissues were scored 1 to 12 according to the IRS method and expressed as Vionlin plot. Mann-Whitney nonparametric test was used to compare the values between tumor tissues and normal tissues ($p < 0.01$).

(B) CD36 IHC staining of A/J mice lungs. A/J mice lung tissue samples from Control and NNK-treated mice (14–16 weeks) were stained for CD36. Bar, 20 μm. The images are representative of three experiments.

(C) The increased CD36 expression and Src/Akt/ERK1/2 kinase activity in the lungs of NNK-induced A/J mice. Proteins from normal lung tissue of the control group and tumors of the NNK group were isolated and pooled from each 3 mice of 14–16 weeks of NNK group and control group. Ctr: normal group lung tissue, NNK: NNK group lung tissue. The relative intensity of protein bands was summarized by column figure. The values indicate the mean ± SD of three independent experiments (Ctr stands for normal group lung tissue, NNK stands for NNK-treated group lung tissue; $^{**}p < 0.01$ vs. Ctr condition, n = 3).

(D) Sarcolemmal CD36 translocation upon NNK treatment. A/J mice lung tissue samples from Control and NNK-treated mice (14–16 weeks) were double stained for CD36 (red) and ATPase (green), respectively. Bar, 10 μm. The images are representative of three experiments.

about the role of CD36 in oral squamous cell carcinoma.[15] We therefore set out to detect CD36 function and the mechanism beyond in the NNK-induced LUAD carcinogenesis.

NNK-upregulated CD36 expression and sarcolemmal distribution were required for NNK-induced lung cell proliferation, migration, and invasion *in vitro*

In light of the association between NNK-upregulated CD36 and LUAD development *in vivo*, we next detect CD36 expression/distribution and lung cell proliferation/invasion upon NNK stimulation *in vitro*. It was found that 0.1–10 μM NNK could induce pro-carcinogenic kinase Akt activation (Figure S1A). 10 μM NNK exerted positive effects on Akt activation in NCI-H23 and Bet1A cells within 60 min (Figure S1B). CD36 expression was upregulated by 10 μM NNK in both cells together with Akt activation (Figure S1C). The time- and dose-dependent experiments of NNK showed that 10 μM NNK could effectively activate Akt in lung cells after 30 min; both Akt activation and CD36 expression reached their peak after 12 h of NNK treatment. Accompanied with NNK-induced CD36 upregulation, α7nAChR expression was confirmed in normal epithelial cell Bet1A and LUAD cells NCI-H23 and A549. NNK increased α7nAChR expression in lung cancer cells NCI-H23 and A549 (Figure 3A). The presence of α7nAChR in NCI-H23, Bet1A, and A549 cells was also demonstrated by RT-PCR (Figures S1D–S1F). Furthermore, there was more surface CD36 upon NNK stimulation (Figure 3B). And NNK-induced CD36 overexpression and sarcolemmal translocation were accompanied by an enhanced lung cell viability (Figure 3C), cell migration (Figures 3D and S2), and cell invasion (Figure 3E) in both NNK-treated NCI-H23 and Bet1A cells. Similar results were obtained in NNK-treated A549 cells (Figures S5A–S5C).

Next, CD36 was knocked down to check whether it could reverse NNK-induced lung cell carcinogenesis. NCI-H23-scramble, NCI-H23-shCD36, Bet1A-scramble, Bet1A-shCD36, A549-scramble, and A549-shCD36 cells were generated (Figures S3 and S5D). Results showed that downregulation of CD36 expression counteracted the NNK-mediated Akt activation (Figure 3F). Importantly, NNK-induced lung cell proliferation (Figures 3G and S5E), cell migration (Figures 3H, S4, and S5F), and cell invasion (Figures 3I and S5G) were inhibited by CD36 knockdown. These changes validated the indispensable role of CD36 in NNK-induced lung carcinogenesis.

NNK activated Akt/ERK via α7nAChR-CD36-Src pathway

The previously described *in vitro* and *in vivo* experiments showed that CD36 was indispensable for NNK-induced lung cell proliferation and metastasis. Given the evidence that NNK could cause lung cell canceration via binding α7nAChR, we next explored whether CD36 was involved in carcinogenic signaling events initiated by α7nAChR. First, α7nAChR inhibitors benzethonium chloride and methylacetonitine citrate were used to treat lung cells for 0.5 and 12 h, respectively. The results showed that these two inhibitors effectively blocked the NNK-induced activation of kinase Src/Akt/ERK1/2 (Figures 4A and S6A). NNK could not activate Src/Akt/ERK1/2 in CD36 knockdown cells (Figures 4B and S6B), the effect was quite similar as α7nAChR inhibitors, suggesting that: 1) NNK induced lung cell carcinogenesis via α7nAChR-CD36 signal pathway; 2) Src/Akt/ERK1/2 kinases located at downstream of α7nAChR and CD36. Next, we set out to clarify the upstream and downstream relationship between Src and Akt/ERK upon NNK stimulation. Src kinase family inhibitor SU6656 and Src kinase inhibitor dasatinib were used to treat lung cells for 0.5 and 12 h,

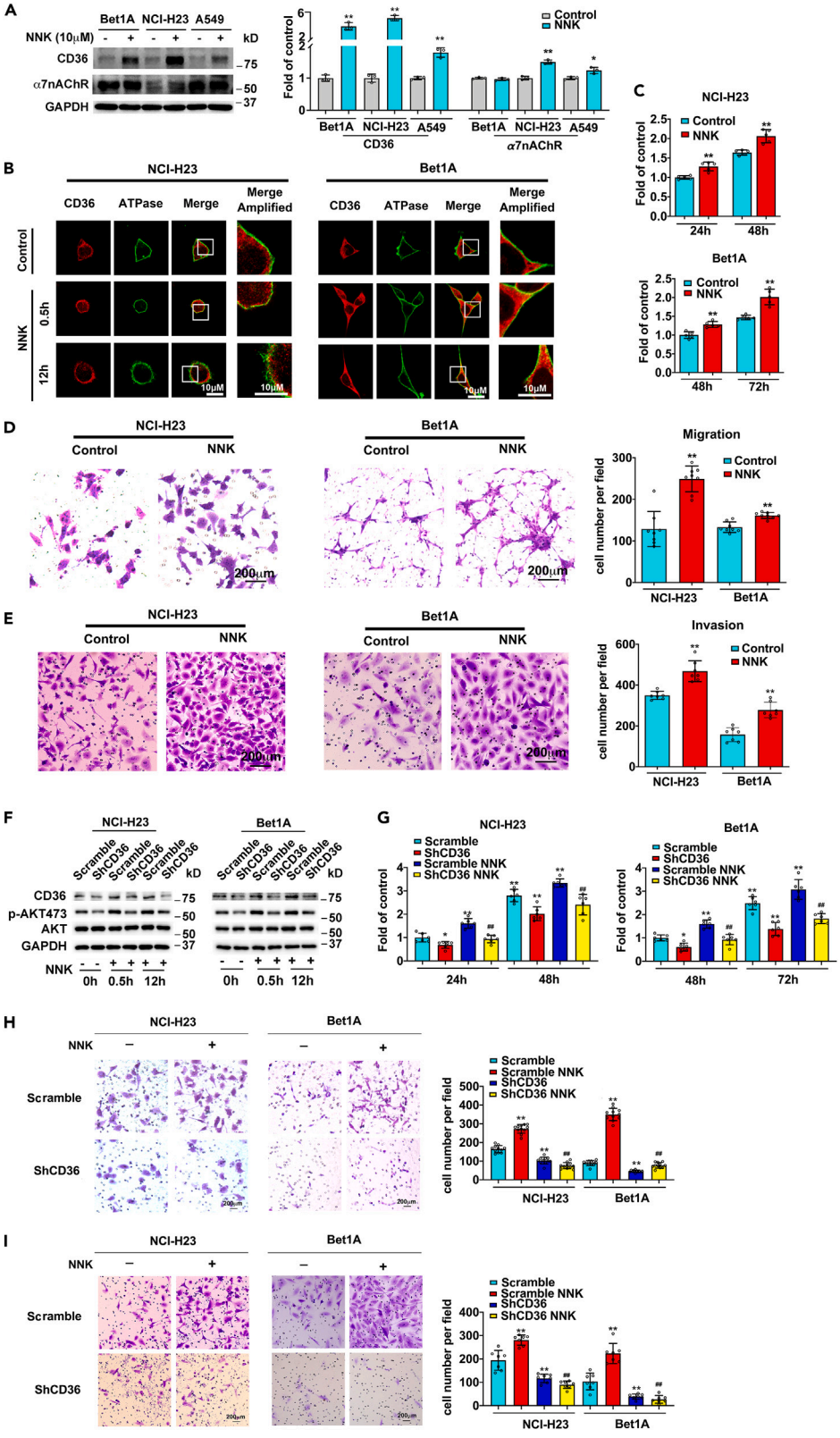
A
Bet1A NCI-H23 A549
NNK (10μM) - + - + - +
kD
CD36
α7nAChR
GAPDH
75
50
37
Fold of control
Control
NNK
Bet1A NCI-H23 A549 Bet1A NCI-H23 A549
CD36
α7nAChR
B
NCI-H23
Bet1A
CD36 ATPase Merge Merge Amplified
Control
NNK
0.5h
12h
10μM
C
NCI-H23
Bet1A
Control
NNK
24h 48h
48h 72h
D
NCI-H23
Bet1A
Control
NNK
200μm
Migration
cell number per field
E
Invasion
F
NCI-H23
Bet1A
Scramble ShCD36 Scramble ShCD36 Scramble ShCD36
CD36
p-AKT473
AKT
GAPDH
NNK
0h 0.5h 12h
G
Scramble
ShCD36
Scramble NNK
ShCD36 NNK
24h 48h
48h 72h
H
NCI-H23
Bet1A
NNK
Scramble
ShCD36
I

Figure 3. NNK upregulated CD36 expression and sarcolemmal distribution were required for NNK-induced lung cell carcinogenesis

(A) Detection of CD36 and α7nAChR expression in lung cells. Bet1A, NCI-H23, and A549 cells were untreated or treated with 10 μM NNK for 12 h. Proteins expression was examined as indicated. Non-NNK treatment cell was set as control. The relative intensity of protein bands was summarized by column figure and expressed as mean ± SD (n = 3, *p < 0.05 and **p < *0.01* vs. Control).

(B) CD36 distribution after NNK stimulation. Bet1A and NCI-H23 cells were untreated or treated with NNK for 0.5 and 12 h, respectively. Cells without NNK treatment were the control. Cells were double stained for CD36 (red) and ATPase (green), respectively. Bar, 10 μm. The images were representative of three experiments.

(C) NNK treatment promoted lung cell viability. Cells treated with 10 μM NNK for different time were used for MTT assay (**p < 0.01, n = 5).

(D and E) NNK induced Bet1A and NCI-H23 cell migration (D) and invasion (E). Cells treated by NNK for 24 h were used for cell migration and invasion assay. Images were taken using phase contrast microscope (Nikon) (scale bar, 200 μm). The numbers of migration or invasion cells in eight randomly selected fields were counted and the average number of cells in one field was calculated and expressed as the mean ± SD (**p < *0.01* vs. Control).

(F) CD36 regulated Akt activation in NNK-treated lung cells. Scramble and ShCD36 cells of Bet1A and NCI-H23 were untreated or treated with NNK as indicated. The levels of CD36 and Akt activity were examined with indicated antibodies.

(G) CD36 was required for maintaining cell viability. Scramble and ShCD36 cells of Bet1A and NCI-H23 were treated with NNK as indicated for MTT assay (*p < *0.05* and **p < *0.01* vs. scramble control; $^{\#}$p < 0.05 and $^{\#\#}$p < 0.01 vs. scramble+NNK, n = 6).

(H and I) CD36 was required for NNK-induced cell migration (H) and invasion (I). Scramble and ShCD36 cells of Bet1A and NCI-H23 treated with NNK for 24 h were detected by *trans*-well experiment for cell migration and invasion, respectively. Images were taken using phase contrast microscope (Nikon) (scale bar, 200 μm). The numbers of migration or invasion cells in eight randomly selected fields were counted and the average number of cells in one field was calculated and expressed as the mean ± SD (*p < *0.05* and **p < *0.01* vs. scramble control; $^{\#}$p < 0.05 and $^{\#\#}$p < 0.01 vs. scramble+NNK).

respectively. The results showed that these two inhibitors effectively blocked the NNK-induced activation of both Src and Akt/ERK1/2 kinase (Figures 4C and S6C), suggesting that Src kinase located upstream of Akt and ERK1/2 to regulate their activity. CD36 knockdown exhibited the similar effects as Src kinase inhibitors since NNK could not activate Src/Akt/ERK1/2 in CD36 knockdown cells (Figures 4D and S6D). These results demonstrated that α7nAChR passed the carcinogenetic signal of NNK to CD36, which in turn activated downstream Akt/ERK via Src kinase.

CD36 functioned as a bridge to link α7nAChR and Src for NNK-induced signal transduction during LUAD carcinogenesis

We then tried to further investigate the relationship among α7nAChR, CD36, and Src. The results previously described showed that more CD36 molecules translocated to the membrane (Figures 2D and 3B), which might be involved in NNK-induced signal transduction. Also, our previous work revealed that palmitic acid (PA) could activate AMPK via surface CD36.[14] When NCI-H23 cells were treated with NNK and PA, respectively, the activity of Src/Akt/ERK1/2 increased, which could be blocked by CD36 inhibitor SSO (Figure 5A). As a fatty acid analog, SSO could bind with the extracellular part of CD36 irreversibly. It has been well documented that PA could induce intracellular signal transduction via sarcolemmal CD36, which could be blocked by SSO. Here, we used PA and SSO as control to demonstrate 1) the inhibition of sarcolemmal CD36 by SSO was successful during NNK stimulation; 2) the CD36 inhibition could counteract NNK-induced signal effectively. Thus, the results confirmed that sarcolemmal CD36 was required for NNK-induced signaling after NNK bound with α7nAChR. How NNK promotes CD36 sarcolemmal translocation still needs further research.

Immunoprecipitation results also showed that it was NNK but not PA that caused the interaction between CD36 and α7nAChR (Figure 5B), which proved that α7nAChR-CD36 interaction was unique to NNK stimulation. Although PA could activate Src/Akt/ERK1/2 via CD36, it was not related to α7nAChR. Consistent with the results that both PA and NNK upregulated Src activation through CD36 (Figure 5A), immunoprecipitation results showed that CD36 interacted with Src upon PA and NNK stimulation, respectively (Figure 5C). However, Src kinase has no direct interaction with α7nAChR (Figure 5D), while Src interacted with CD36 under PA and NNK treatment (Figure 5E). Thus, CD36 could colocalize with α7nAChR and Src kinases in the presence of NNK. Immunofluorescence (IF) results further verified these colocalization. CD36/α7nAChR and CD36/Src dispersed in the cells in basal condition, while NNK enhanced their colocalization, especially on the plasma membrane (Figures 5F and 5G). However, there was a weaker colocalization between α7nAChR and Src upon NNK treatment (Figure 5H). Therefore, the immunoprecipitation and IF results suggested that CD36 might interact with α7nAChR and Src directly while α7nAChR and Src are spatially close to each other through

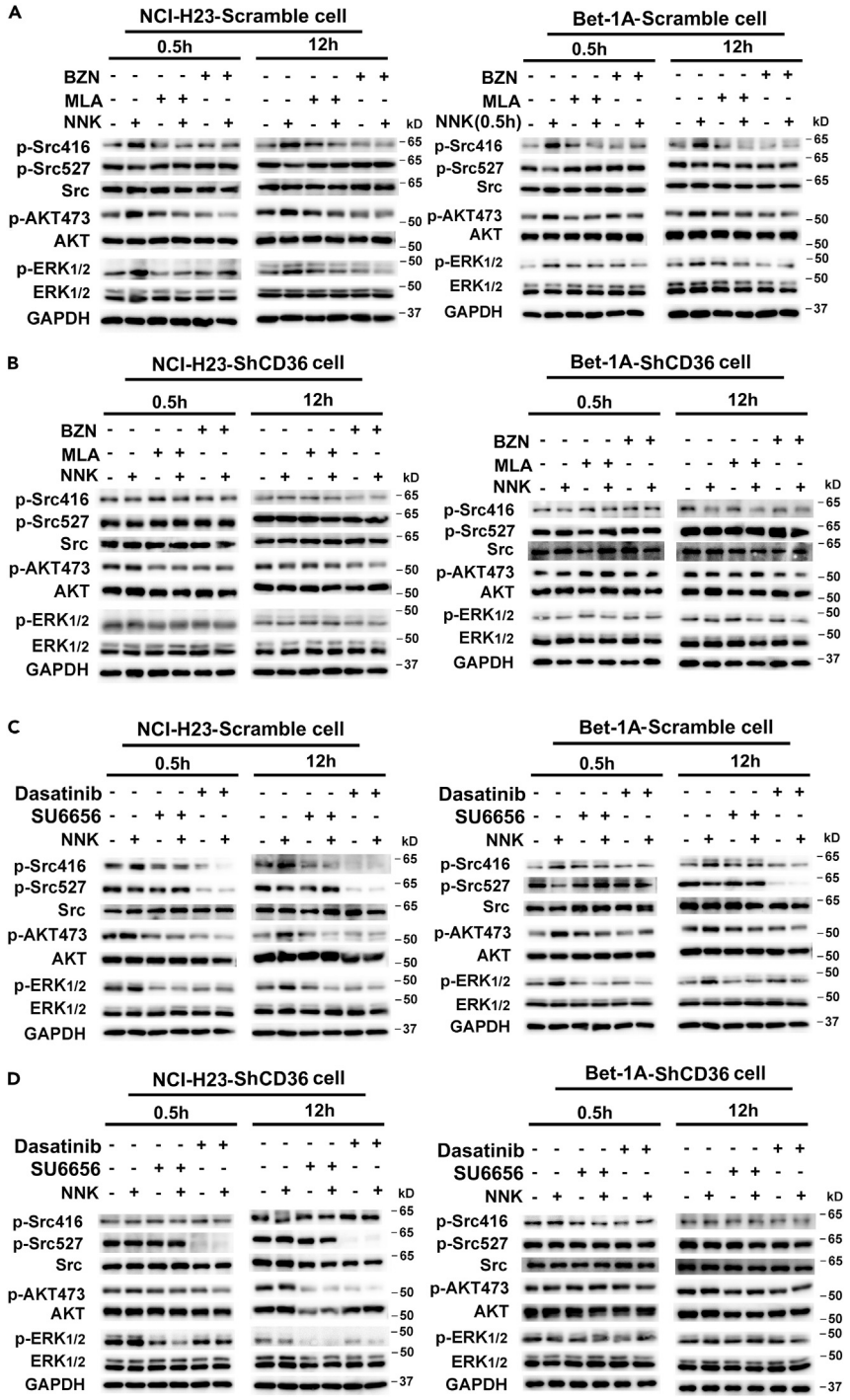

Figure 4. NNK activated Akt/ERK1/2 via α7nAChR-CD36-Src pathway

(A and B) NNK activated Src/Akt/ERK1/2 through α7nAChR (A) and Effect of CD36 knockdown was similar as α7nAChR inhibitors (B).

The constructed cells as indicated in the figures were untreated or treated with 10 μM NNK, or cells were pretreated with 1 μM α7nAChR receptor inhibitor benzethonium chloride (BZN) or 10 μM α7nAChR receptor inhibitor methylacetonitine citrate (MLA) for 30 min, which was followed by 10 μM NNK treatment for another 0.5 or 12 h, respectively. Untreated cells were set up as controls. Proteins expression and activity were determined by western blot.

(C and D) NNK activated Akt/ERK1/2 through Src kinase (C) and Effect of CD36 knockdown was similar as Src inhibitors (D).

Figure 4. *Continued*
The constructed cells as indicated in the figures were untreated or treated with 10 μM NNK, or cells were pretreated with 10 μM Src kinase family inhibitor SU6656 or 100 nM Src kinase inhibitor dasatinib for 30 min, which was followed by 10 μM NNK treatment for 0.5 or 12 h, respectively. Untreated cells were set up as controls. Proteins expression and activity were determined by western blot.

CD36. We concluded that NNK promoted the migration of CD36 to cell membrane, where CD36 colocalized with α7nAChR and Src simultaneously. CD36 functioned as a bridge between α7nAChR and Src to mediate NNK-induced activation of Src and downstream kinases Akt and ERK1/2.

CD36 was required for NNK-induced tumorigenic properties of LUAD cells

To confirm the tumor-essential function of CD36 *in vivo*, we first generated subcutaneous xenograft models. In Figure 6A, the mean tumor volume derived from A549-scramble-NNK cells was 2.3-fold of A549-scramble ($p < 0.05$). In contrast to A549-scramble control, A549-shCD36 exhibited markedly decreased growth of only 0.15-fold of A549-scramble ($p < 0.01$). Though the mean tumor volume derived from A549-shCD36-NNK cells was larger than that of A549-shCD36 ($p < 0.01$), the knockdown of CD36 counteracted the NNK effect on induction of tumor growth because the mean tumor volume formed was only 0.5-fold of A549-scramble ($p < 0.05$) and 0.2-fold of A549-scramble-NNK ($p < 0.01$), respectively. Pathologic analysis revealed that relative to A549-scramble tumors, A549-scramble-NNK tumors were poorly differentiated, more aggressive, and contained highly heterogeneous cell types (spindle cells, cells with high nuclear-cytoplasm ratio, and mitotic cells). Whereas, A549-ShCD36 and even A549-ShCD36-NNK tumors retained well-differentiated glandular structures with more loosely arranged cells, when compared with A549-scramble and A549-scramble-NNK tumors (Figure 6B). These pathologic differences among tumors were accompanied with the different levels of CD36 expression (Figure 6C). Consistent with these, there were higher CD36 expression and increased activity of Src/Akt/ERK1/2 in A549-scramble-NNK tumor when compared with A549-scramble tumor samples (Figure 6D). While in tumors derived from A549-shCD36 cells, downregulation of CD36 expression significantly counteracted the NNK-induced activation of Src/Akt/ERK1/2 (Figure 6D).

To investigate oncogenic effect of CD36 on LUAD metastasis, the A549-scramble, A549-scramble-NNK, A549-shCD36, and A549-ShCD36-NNK cells were inoculated into nude mice via tail-vein injection. The mice were sacrificed 12 weeks later to examine metastatic nodules in lung, liver, and spleen. The results in Figure 6E showed that the mean metastatic number of nodules derived from A549-scramble-NNK cells was higher than that of A549-scramble cells ($p < 0.01$). In contrast to A549-scramble control, A549-shCD36 exhibited markedly decreased metastatic nodules in the xenograft model ($p < 0.01$). And knockdown of CD36 in A549-shCD36-NNK cells counteracted the NNK effect on tumor cell metastasis ($p < 0.01$), suggesting that CD36 was key to promote LUAD cells metastasis. Pathologic analysis revealed that, compared with A549-scramble tumors, the A549-scramble-NNK tumors have already well developed and the size of the tumors was larger. Whereas, A549-ShCD36 cells injection did not form tumors in the lung, and A549-ShCD36-NNK in mice was still in neoplasia stage (Figure 6F). We did not find metastatic nodules in the liver and spleen of nude mice (data not shown). The IHC staining of lungs in Figure 6G indicated that CD36 expression of the tumor cells was higher than that of the normal lung cells adjacent to the tumor. Specially, the margin cells of these well-developed tumors contained higher level of CD36, suggesting that these cells might possess higher metastasis potential. A549-ShCD36 cells injection could not form lung tumors and CD36 expression level was normal in the lung cells. Neoplasia cells with higher CD36 expression could be found in the A549-ShCD36-NNK group. The results indicated that CD36 expression level in A549 cells positively related to metastatic tumor formation. Similar results were obtained for NCI-H23 cells (Figure S7), which showed that the mean volume of tumors formed by NCI-H23-scramble-NNK cells was significantly larger than that of NCI-H23-scramble control ($p < 0.05$). Intriguingly, CD36 knockdown in NCI-H23 cells did not form subcutaneous tumors, even after NNK treatment. Since 28 days of NNK treatment were not long enough to make cancer stem cells-like Bet1A cells tumorigenically stable enough to generate tumors,[25] we did not employ Bet1A cells for the *in vivo* detection. Taken together, these findings demonstrated that CD36 was indispensable for the tumorigenic properties of LUAD cells and NNK-induced LUAD development.

CD36 inhibitor SSO inhibited LUAD cell metastasis *in vivo*

To further evaluate the potential therapeutic effect of targeting CD36 on LUAD cell metastasis, SSO, an irreversible chemical inhibitor of CD36, was used. A549-control, A549-SSO, A549-NNK, and A549-NNK-SSO cells were inoculated into nude mice via tail-vein injection, respectively. As shown in Figures 7A

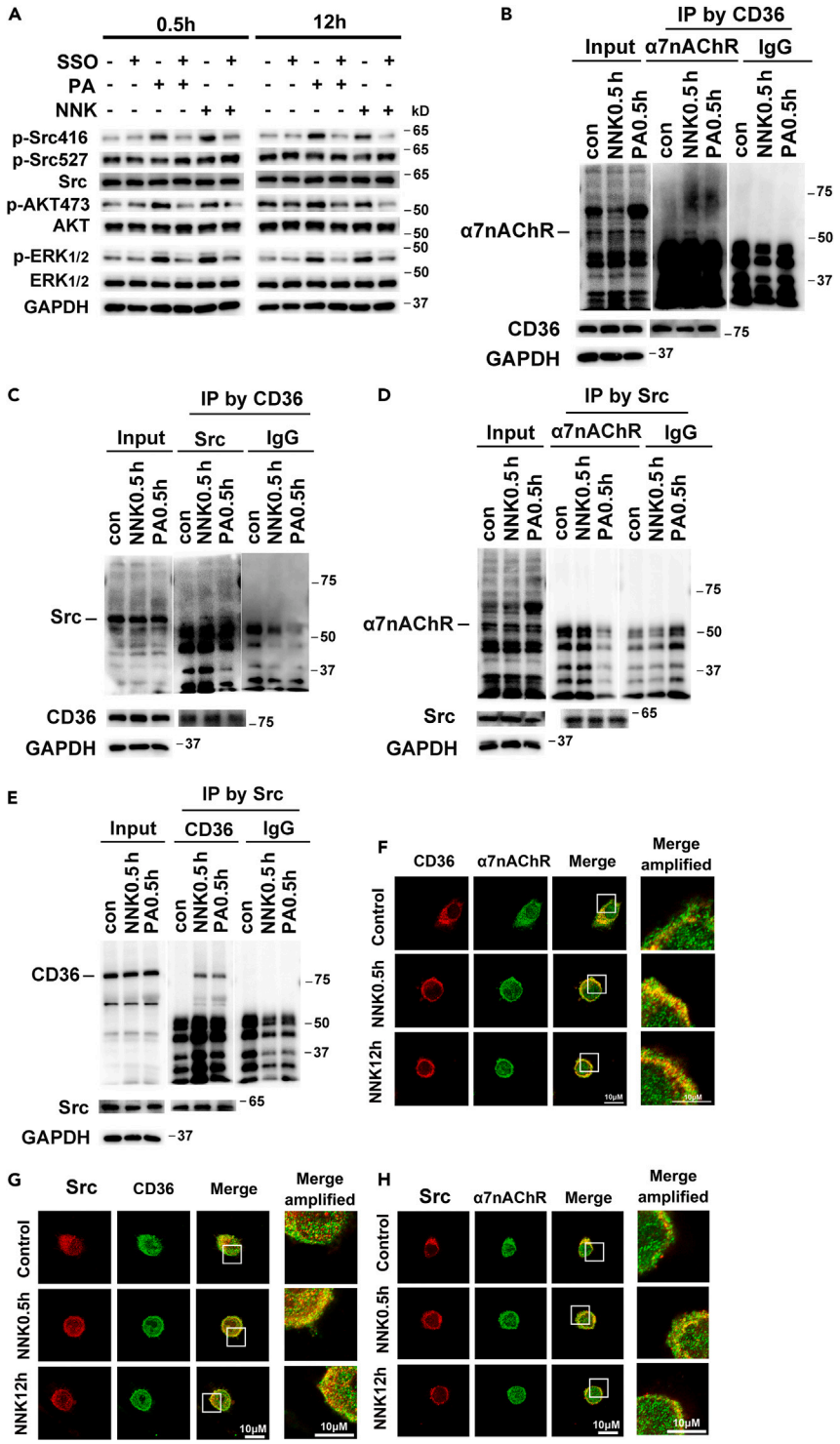

Figure 5. CD36 interacted with both α7nAChR and Src to mediate NNK-induced signaling during LUAD carcinogenesis

(A) CD36 inhibitor SSO blocked NNK- and PA-induced activation of Src/Akt/ERK1/2. NCI-H23 cells were untreated or treated with 10 μM NNK, or cells were pretreated with 200 μM SSO (a fatty acid analog as CD36 blocker) for 30 min, which was followed by 10 μM NNK or 500 μM PA treatment for 0.5/12 h. Untreated cells were set up as controls. Proteins expression and activity were determined by western blot.

Figure 5. *Continued*

(B–E) Examination of the interaction among α7nAChR, CD36, and Src by immunoprecipitation. Briefly, NCI-H23 cells were treated with 10 μM NNK or 500 μM PA for 0.5 h. Untreated cells were set up as controls. Total cell lysis (input) was detected with indicated antibodies. CD36 immunoprecipitates (IP by CD36 antibody) were examined with (B) α7nAChR and (C) Src antibodies, respectively; Src immunoprecipitates (IP by Src antibody) were examined with (D) α7nAChR and (E) CD36 antibodies, respectively.

(F–H) Examination of the colocalization among α7nAChR, CD36, and Src by immunostaining. Briefly, NCI-H23 cells were untreated or treated with 10 μM NNK for 0.5 or 12 h. Untreated cells were set up as controls. The fixed cells were double stained for (F) CD36 (red) and α7nAChR (green); (G) Src (red) and CD36 (green); and (H) Src (red) and α7nAChR (green), respectively. Bar, 10 μm. The images were representative of three experiments.

and 7B, SSO did not produce cell cytotoxicity and significantly inhibited the NNK-induced LUAD cell proliferation. It should be noted that the SSO concentration here was lower than that in Figure 5. The principle of SSO application in our experiment is to try to get significant inhibition effect while minimizing concentration and duration of treatment as much as possible. Furthermore, inhibition of CD36 by SSO significantly decreased the NNK-induced A549 cells to form metastatic LUAD tumors on the lung in nude mice (Figure 7C), indicating the CD36 inhibitor could be a potential drug for LUAD treatment. Injecting SSO to block the effect of NNK *in vivo* still needs further research. Pathologic analysis showed the A549-NNK-SSO cells exhibited less pulmonary metastatic tumors when compared with that of A549-NNK cells, and A549-SSO cells injection did not form lung tumors (Figure 7D). The IHC staining of lungs (Figure 7E) indicated that CD36 expression of the tumor cells was higher than that of the normal lung cells adjacent to the tumors. The results indicated that CD36 inhibitor SSO inhibited LUAD cell metastasis in vivo.

$CD36^{-/-}$ A/J mice counteracted NNK-induced LUAD tumor formation

Next, we went further to confirm the role of CD36 in NNK-induced LUAD tumor formation *in vivo*. A/J mouse is a suitable model to study NNK-induced lung adenocarcinoma. However, it is difficult to perform gene knockout on A/J mouse while it is easy to knockout genes in C57BL/6J mice. In this case, we created a brand-new $CD36^{-/-}$ A/J mouse model to investigate CD36 function by mating $CD36^{+/-}$ C57BL/6J mice with $CD36^{+/+}$ A/J mice. CD36 knockout did not affect reproduction when compared with $CD36^{+/+}$ A/J mice. The CD36 gene was knockout as indicated in Figure S8A. Ear samples from different CD36 genotype C57BL/6J mice were examined by PCR (Figures S8A and S8B). CD36 expression in different tissues of $CD36^{+/+}$ (wild type, WT) and $CD36^{-/-}$ (knockout, KO) C57BL/6J mice were examined to demonstrate CD36 KO successfully (Figure S8C). The $CD36^{+/-}$ C57BL/6J mice were back-crossed with WT A/J mice for five generations to produce $CD36^{+/-}$ mice with A/J background (96.87% homozygosity of A/J mice) (Figures 8A and S8D; Table S3). The ear samples from different CD36 genotype A/J mice were examined by PCR (Figure 8B). CD36 protein was detected in different tissues of $CD36^{+/+}$ (WT) and $CD36^{-/-}$ (KO) A/J mice to confirm CD36 KO successfully (Figure S8E). Compared with $CD36^{+/+}$ A/J mice, NNK injection induced obviously less LUAD tumors on the lungs of $CD36^{-/-}$ A/J mice (Figure 8C). NNK-induced lung adenocarcinoma was also tested in $CD36^{+/+}$ and $CD36^{-/-}$ male A/J mice (Figure S8F). The tendency of the result was quite similar as females (Figure 8C). Pathologic analysis confirmed that the NNK-treated $CD36^{-/-}$ A/J mice exhibited a significantly decreased LUAD tumor formation when compared with that of NNK-treated $CD36^{+/+}$ A/J mice (Figure 8D). Consistently, in the lungs of $CD36^{+/+}$ A/J mice, NNK treatment significantly increased CD36 expression and induced more tumors (Figure 8E). However, in the lungs of $CD36^{-/-}$ A/J mice, there was no CD36 protein and NNK could not produce more tumors as it did in $CD36^{+/+}$ mice (Figure 8E).

DISCUSSION

Cigarette smoking derivative NNK has been identified as a potent pulmonary carcinogen, independent of the route and type of administration.[27] The amount of NNK in one stick of cigarette ranges between 16 and 369 ng,[28] and the NNK concentration produced by one pack of cigarettes in the body is about 7 μM.[29] NNK or its metabolites can be chronically deposited locally in large amount without producing pulmonary cytotoxicity.[30] Considering these facts and our previous study,[25,31] and also the dose-response curve of NNK obtained in the present study, 10 μM NNK was used for *in vitro* experiments. α7nAChR is widely expressed in lung cancer cells and implicated as the primary receptor facilitating NNK-mediated cell proliferation through engaging various signal transduction molecules and transcription factors.[7] The cells applied in this work all contained α7nAChR (Figures 3A and S1D–S1F).

In recent decades, CD36 has been found to be related to metastasis, metabolism, and chemotherapy resistance of several types of tumor cells,[15,32,33] but little is known about the role of CD36 in LUAD cells. Here,

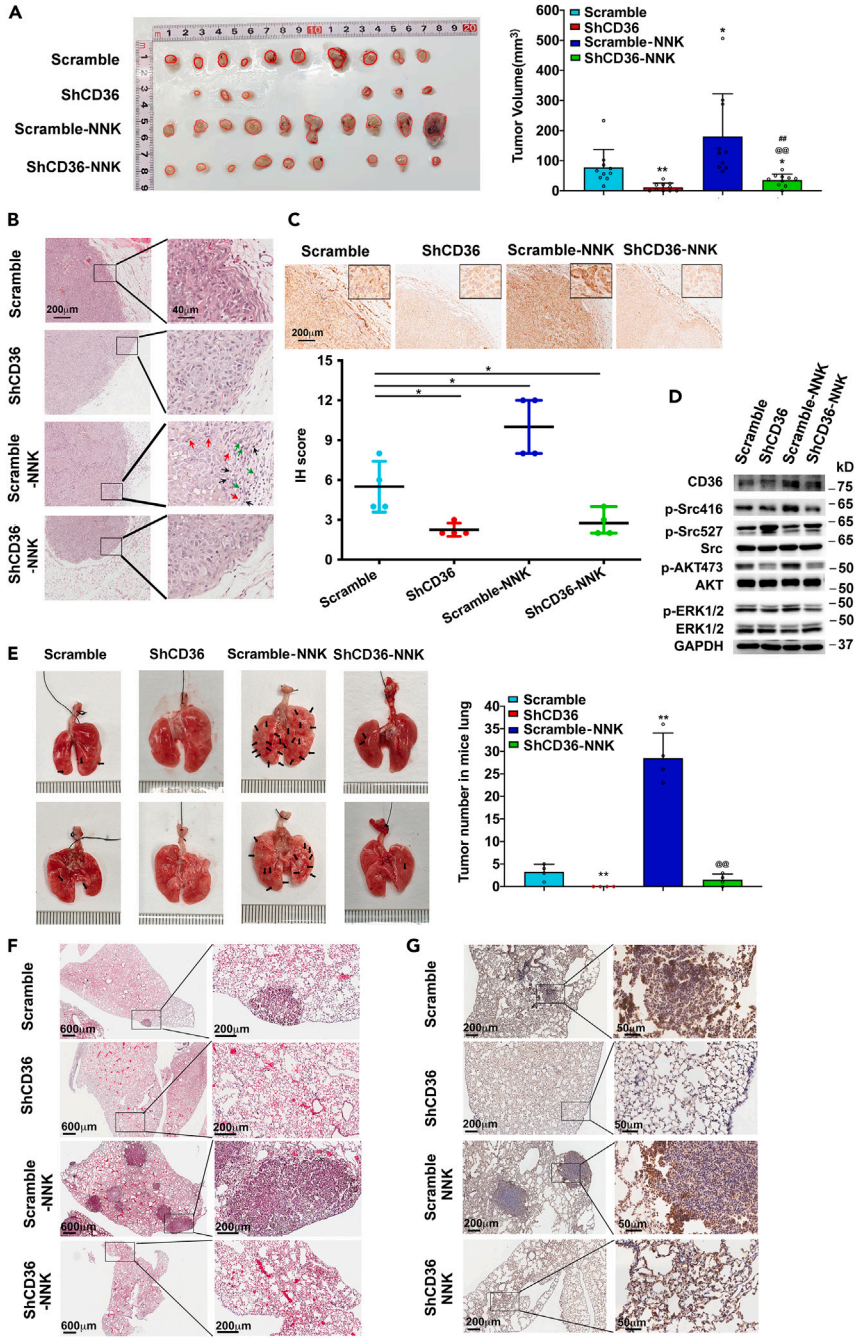

Figure 6. Downregulation of CD36 expression inhibited NNK-induced LUAD tumor growth and metastasis in xenograft mouse models

(A) CD36 knockdown in LUAD cells inhibited xenograft tumor growth. The nude mice were subcutaneously transplanted with A549-scramble, A549-scramble-NNK, A549-ShCD36, or A549-ShCD36-NNK cells, respectively. The tumor was collected 6 weeks later and the size of tumor was measured (n = 10, *p < *0.05 and* **p < *0.01* vs. Scramble; $^{\#\#}$p < *0.01* vs. ShCD36; $^{@@}$p < *0.01* vs. Scramble-NNK).

(B) CD36 knockdown in LUAD cells inhibited xenograft tumor aggressiveness. Sections of the xenograft tumor generated by A549-scramble, A549-cramble-NNK, A549-ShCD36, or A549-ShCD36-NNK cells were stained with H&E and examined. Note the poorly differentiated and more aggressive cells in A549-scramble-NNK tumors (Spindle cells (red arrows), cells with high nuclear-cytoplasm ratio (green arrows), mitotic cells (black arrows)) were indicated. Bar: 200 and 40 μm, respectively.

Figure 6. *Continued*

(C) CD36 IHC staining in the xenograft tumors. Immunohistochemical analysis of tumors with antibodies against CD36 was performed. IH-scores for CD36 were calculated for tumors, and the results represent the mean ± SD of four individual tumors per group (*p < *0.05*). Bar: 200 μm.

(D) CD36 knockdown inhibited Src/ERK1/2/Akt activation in xenograft tumor tissues. Five of each group of xenograft tumor tissue proteins was pooled together and the indicated protein expression and activity in the xenografts were detected.

(E) Detection of lung metastasis of tail-vein injected LUAD cells. Lungs of nude mice 12 weeks after tail-vein injection of A549-scramble, A549-scramble-NNK, A549-ShCD36, or A549-ShCD36-NNK cells were collected. Gross appearance and total number of metastatic nodules in lungs of nude mice were analyzed. Arrows indicated nodules formed on the lungs. Nodule numbers of individual mouse for each group were counted and summarized by the column figure. Data were mean ± SD (*p < *0.05 and* **p < *0.01* vs. Scramble; $^{@@}$p < *0.01* vs. Scramble-NNK; n = 4).

(F) Pathologic analyses of the lungs after tail-vein injection of LUAD cells. Lung tissue sections from mice of A549-scramble, A549-scramble-NNK, A549-ShCD36, or A549-ShCD36-NNK group were stained with H&E and examined. Bar: 600 and 200 μm, respectively.

(G) IHC staining of the lungs after tail-vein injection of LUAD cells. Lung tissue sections from mice of A549-scramble, A549-ShCD36, A549-scramble-NNK, or A549-ShCD36-NNK group were stained with CD36 antibody and examined. Bar: 200 and 50 μm, respectively.

the overall CD36 expression level was demonstrated to be higher in human LUAD tumor tissues than that in the adjacent normal lung tissues (Figures 1A–1C). The level of CD36 was also higher in NNK-induced A/J mice LUAD tumor tissues than that in the normal A/J mice lung tissues (Figures 2A–2C). Importantly, higher CD36 level positively related to human LUAD metastasis (Figure 1D). The tail-vein injection experiment also exhibited higher CD36 expression in tumors formed by the metastatic LUAD cells (Figure 6G). Thus, CD36 can be used as a marker of cells with the ability to initiate tumor metastasis.[15] We notice there is a report showing that CD36 expression is lower in LUAD cells when compared with the para-tumor cells (but not the adjacent normal lung cells).[34] According to the image shown in that paper, the most probability of this discrepancy from our findings may be due to their statistical difference calculated by selection of para-tumor cells but not the adjacent normal lung cells. It is worth mentioning that NNK could still exhibit carcinogenetic effect even in CD36 KO A/J mice, but the number of NNK-induced tumor was significantly reduced (Figure 8). The most probability is that NNK could diffuse through the cell membrane and induce DNA adducts to activate mutations in proto-oncogenes and inactivate tumor suppressor genes. And more, NNK and its metabolites in the lung cell could activate some targets, such as TCTP, 15-LOXs PPARγ, and HO-1, to promote lung cell carcinogenesis.[25,26,31,35] Obviously, the signaling events induced by NNK through α7nAChR-CD36 have a significant contribution to the carcinogenic process.

Our study proved that NNK could induce CD36 translocation to plasma membrane (Figures 2D and 3B), where it colocalized with α7nAChR and Src (Figures 5B, 5C, and 5E–5G). Yet there is no obvious colocalization between α7nAChR and Src after NNK treatment (Figures 5D and 5H). How NNK induces CD36 sarcolemmal translocation still needs further research. Our work revealed for the first time that CD36 functioned as a bridge between α7nAChR and Src to mediate NNK-induced signal transduction during LUAD development. α7nAChR inhibitors, CD36 knockdown, and CD36 antagonist SSO could block NNK-induced activation of Src, which indicated that α7nAChR initiated a CD36-dependent tumorigenic signal after binding with NNK and CD36 located upstream of Src kinase (Figures 4 and 5A). Indeed, the upregulated CD36 expression exhibited a positive correlation with Src activity in LUAD specimens (Figures 1C and 2C). Our finding is consistent with a previous work on cervical cancer which demonstrates that upregulation of Src pathway by CD36 is a potential mechanism to induce cell growth and metastasis.[36] Also, the engagement of CD36 causes activation of Src family kinases, such as Fyn and/or Lyn, resulting in actin polymerization, loss of cell polarity, and increased cell spreading.[14,37] In the future study, it is worth to explore how α7nAChR interacts with surface CD36 to transmit NNK signal.

Combined with our previous report that CD36 mediates cellular fatty acid uptake,[14] the results here reveal a dual role of CD36 in NNK-induced LUAD development after CD36 sarcolemmal translocation. In one hand, CD36 acts as a bridge between α7nAChR and Src to transmit the information of NNK, because CD36 knockdown LUAD cells and CD36 KO A/J mice could counteract the NNK-induced LUAD tumor formation and metastasis (Figures 6 and 8). On the other hand, CD36 may initiate signal transduction to help cells to uptake fatty acids, since fatty acid uptake and lipid metabolism are essential cellular processes to promote tumorigenesis and tumor progression.[38] Indeed, CD36 knockdown and CD36 irreversible inhibitor SSO significantly inhibited tumor growth and metastasis in the xenograft model (Figures 6, 7C–7E, and S7). Thus, CD36 plays important roles in the development of cancer through different mechanisms.[15,39] Both PA and NNK could activate Src/Akt/ERK1/2 kinase (Figure 5A). The CD36 blocker SSO effectively eliminated the effect of both PA and

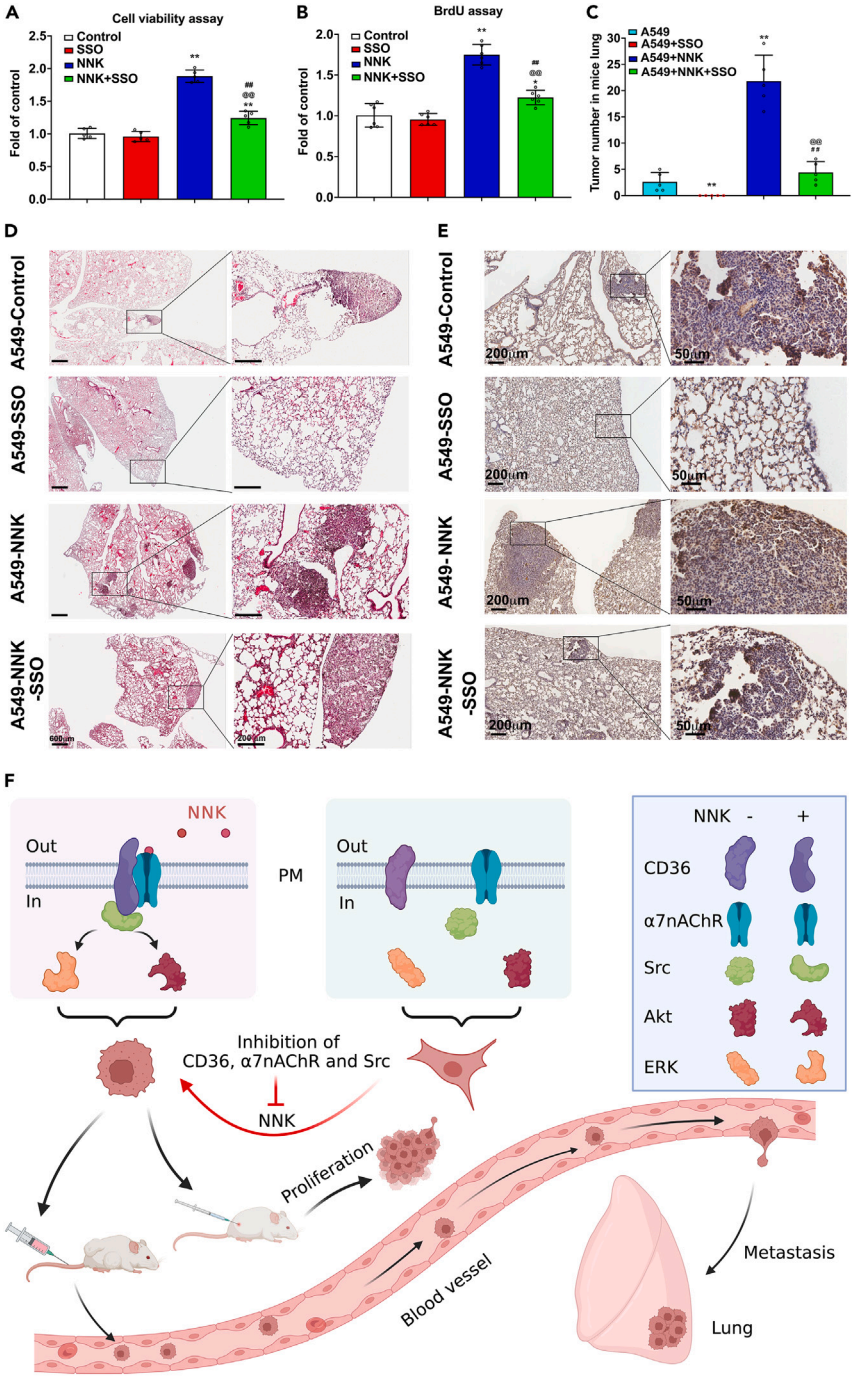

Figure 7. SSO treatment inhibited LUAD cell metastasis *in vivo*

A549 cells were treated with or without 10 μM NNK for 28 days, or cells were treated with 50 μM SSO for 28 days, or cells were treated with 50 μM SSO plus 10 μM NNK for 28 days. Then the cells were applied for the following experiments.

(A) SSO inhibited NNK-enhanced LUAD cell viability. The cells were seeded in 96-well plate and MTT assay was performed. Non-treatment condition was set up as 1, $^{**}p < 0.01$ vs. control, $^{\#\#}p < 0.01$ vs. NNK+SSO, $^{@@}p < 0.01$ vs. SSO, n = 5.

(B) SSO inhibited NNK-induced LUAD cell proliferation. The cells were applied for BrdU assay. Non-treatment condition was set up as 1, $^{*}p < 0.05$ and $^{**}p < 0.01$ vs. control, $^{\#\#}p < 0.01$ vs. NNK+SSO, $^{@@}p < 0.01$ vs. SSO, n = 6.

(C) SSO treatment inhibited NNK-induced LUAD cell metastasis *in vivo*. Cells were injected into nude mice through tail-vein and the mice were killed after 12 weeks. The lung metastatic nodules were calculated. Data were mean ± SD, $^{**}p < 0.01$ vs. A549, $^{\#\#}p < 0.01$ vs. A549+NNK. $^{@@}p < 0.01$ vs. A549+SSO, n = 5.

Figure 7. *Continued*

(D) Pathologic analyses of the lungs after tail-vein injection of LUAD cells. Lung tissue sections from mice of A549, A549-NNK, A549-SSO, or A549-SSO-NNK group were stained with H&E and examined. Bar: 600 and 200 μm, respectively.
(E) IHC staining of the lungs after tail-vein injection of LUAD cells. Lung tissue sections from mice of A549, A549-NNK, A549-SSO, or A549-SSO-NNK group were stained with CD36 antibody and examined. Bar: 200 and 50 μm, respectively.
(F) Schematic mechanism illustrating the NNK-induced LUAD cell proliferation and metastasis. Upon NNK binding with α7nAChR, sarcolemmal CD36 interacted with surface α7nAChR and cytosol Src simultaneously, which led to activation of Src and downstream pro-carcinogenic kinase ERK and Akt. CD36 exhibited obvious tumorigenic function during NNK-induced LUAD cells to form subcutaneous and pulmonary metastatic tumors. NNK/α7nAChR-mediated lung cell proliferation and metastasis could be counteracted by inhibition of CD36, α7nAChR, and Src.

NNK, suggesting that PA, like NNK, may also facilitate LUAD cell proliferation via CD36 (Figure 5A). Many studies have shown that the changes of lipid metabolism are closely related to the occurrence of tumor.[40] $CD36^{+}$ tumor stem cells have unique metabolic characteristics and can carry out self-renewal, initiate tumor metastasis, and resist chemotherapy.[15] Dietary oleic acid exerts a stimulatory effect on cervical cancer growth and metastasis by inducing Src kinase and downstream ERK1/2 pathway activation in a CD36-dependent manner.[36] Akt is crucial for the regulation of glycolysis.[41] CD36 induces mTOR-mediated oncogenic glycolysis via activation of Src/PI3K/Akt signaling axis and exerts a stimulatory effect on HCC growth and metastasis.[42] These findings demonstrate that LUAD cells need to uptake more fatty acid through surface CD36 to meet the energy needs of tumor cell proliferation, migration, and infiltration. And NNK-induced CD36 relocation on plasma membrane might mediate the effect of both NNK and PA. How NNK exhibits its carcinogenic effect in a high-fat environment still needs further research.

Src locates in the cytosol and transduce signals between cell surface proteins and intracellular proteins.[43] Under physiologic conditions, Src is normally maintained in an inactive state via phosphorylation of negative regulatory C-terminal Tyr $^{(527/530)}$ site of the protein.[24] Dephosphorylation of this site changes Src conformation and results in the autophosphorylation of Tyr $^{(416/419)}$ within the activation loop of Src protein, leading to Src be fully activated and interacts with other proteins.[43] Our study proved that NNK-induced Src activation indicated by dephosphorylation at Tyr^{527} and phosphorylation at Tyr^{-416}. Increased activity of Src has been reported in 60%–80% of patients with LUAD.[44] And the NSCLC cell lines had the highest median Src activity among 60 cancer cell lines studied.[45] Several studies show that the mitogenic effects of nicotine in NSCLC cells involve the Src activation: nicotine mainly acts on α7nAChR to induce NSCLC tumor cell proliferation by the activation of Src and Rb-Raf-1 pathways[46]; nicotine-activated Src kinase upregulates mesenchymal genes and ZEB1 and ZEB2[47]; NNK-induced migration and invasion may occur in a mechanism through activation of a c-Src loop[21]; and dasatinib induces apoptosis in NSCLC cells by blocking the activation of c-Src.[48] In the downstream of Src, there are two major cell survival and growth signaling pathways, namely PI3K/Akt and Ras-Raf-ERK1/2 pathways, resulting in a generation of mitogenic and tumorigenic signals.[20] In our work, we also examined the correlation between Src and Akt/ERK1/2. The results indicated that Src located upstream of Akt and ERK1/2, and controlled their activity upon NNK stimulation (Figure 4). Thus, NNK could activate Akt/ERK1/2 via α7nAChR-CD36-Src pathway.

Collectively, we demonstrated that CD36 participated in the occurrence and development of LUAD upon NNK stimulation. NNK promoted LUAD cell proliferation, migration, and invasion in a CD36-dependent manner after binding to α7nAChR (Figure 7F). Targeting CD36 and α7nAChR-CD36-Src signal axis may provide a breakthrough therapy during the carcinogenic process of LUAD.

Limitations of the study

While the present study reveals NNK promotes LUAD cell proliferation, migration, and invasion in a CD36-dependent manner, there are several limitations that should be considered. First, there are less female LUAD patients recruited in our database; this might cause bias to evaluate the relationship between smoking-related CD36 expression and gender here. It is still necessary to recruit more female patients in future studies. Second, the mechanism of CD36 sarcolemmal translocation upon NNK stimulation remains to be explored. Third, how CD36 interacts with α7nAChR on the plasma membrane is to be clarified. Further studies are needed to gain a comprehensive understanding of these points.

STAR★METHODS

Detailed methods are provided in the online version of this paper and include the following:

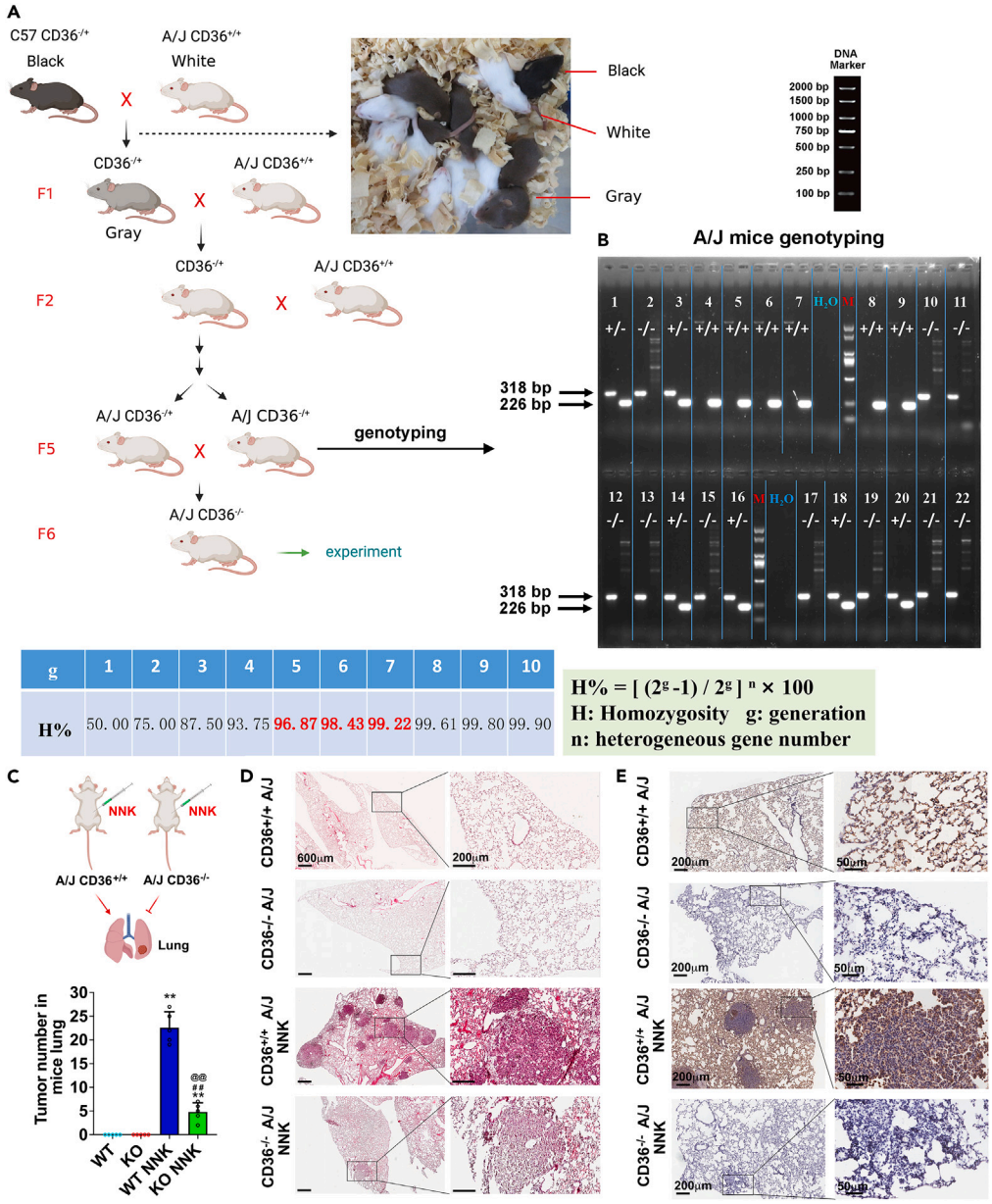

Figure 8. CD36$^{-/-}$ A/J mice counteracted NNK-induced LUAD tumor formation

(A) Construction of CD36$^{+/-}$ A/J background mice. CD36$^{+/-}$ C57BL/6 mice were backcrossed to A/J mice for five generations to generate CD36$^{+/-}$ A/J background mice. The homozygosity of A/J background mice by back-crossed five generations was 96.87%.

(B) F5 A/J mice genotyping by PCR. No. 4–9 mice obtained a 226 bp band as CD36$^{+/+}$ wild type. No. 1, 3, 14, 16, 18, and 20 mice obtained both 226 and 318 bp bands as CD36$^{+/-}$ genotype. No. 2, 10, 11, 12, 13, 15, 17, 19, 21, and 22 mice obtained a 318 bp band as CD36$^{-/-}$ genotype.

(C) CD36$^{-/-}$ A/J mice counteracted NNK-induced LUAD tumor formation. The WT (CD36$^{+/+}$) and KO (CD36$^{-/-}$) A/J mice were injected intraperitoneally (ip) with either NNK (100 mg/kg) or equivalent volume of physiological saline. Mice were humanely culled 16 weeks later and the lung nodules were calculated. (**p < *0.01* vs. WT; $^{\#\#}$p < *0.01* vs. WT NNK; $^{@@}$p < *0.01* vs. KO).

(D) Pathologic analyses of the lungs in A/J mice. Lung tissue sections from WT (CD36$^{+/+}$), KO (CD36$^{-/-}$), WT (CD36$^{+/+}$)-NNK, and KO (CD36$^{-/-}$)-NNK A/J mice group were stained with H&E and examined. Bar: 600 and 200 μm, respectively.

(E) IHC staining of the lungs in A/J mice. Lung tissue sections from WT (CD36$^{+/+}$), KO (CD36$^{-/-}$), WT (CD36$^{+/+}$)-NNK, or KO (CD36$^{-/-}$)-NNK A/J mice group were stained with CD36 antibody and examined. Bar: 200 and 50 μm, respectively.

- KEY RESOURCES TABLE
- RESOURCE AVAILABILITY
  - Lead contact
  - Materials availability
  - Data and code availability
- EXPERIMENTAL MODEL AND SUBJECT DETAILS
  - LUAD cancer sample collection
  - Animal treatment
  - Cell culture
  - Transient transfection and establishment of stable cell lines
  - Xenograft model
- METHODS DETAILS
  - The OS (overall survival) analysis by Kaplan–Meier plotter software
  - Western-blot
  - Immunohistochemistry (IHC), immunofluorescence (IF) and haematoxylin-eosin (H&E) staining
  - Quantitative RT-PCR
  - F5 A/J mice genetic background detection
  - Assessment of cell viability
  - Wound healing and transwell assay
  - Co-immunoprecipitation (Co-IP)
- QUANTIFICATION AND STATISTICAL ANALYSIS

SUPPLEMENTAL INFORMATION

Supplemental information can be found online at https://doi.org/10.1016/j.isci.2023.107477.

ACKNOWLEDGMENTS

We thank Mr. Rocky Ho, Mr. Ernest Chak, and Miss Angel Kong (The Chinese University of Hong Kong) for their technical assistance. This study was supported by grants from the National Natural Science Foundation of China (No: 82072584), Shenzhen University Stability Support Plan (20200813175957001), Shenzhen Basic Research General Project (20220523193414003), and CUHK Research Committee Direct Grant of the Hong Kong SAR 2017.081.

AUTHOR CONTRIBUTIONS

Conception and design: L.Z.L. and M.Y.L.; Experiments: M.W., M.D., Z.W., R.Z., B.W., Y.H., X.Z., J.Z., and J.Y.; Statistical analysis: M.Y.L. and L.Z.L.; Analysis and interpretation of data: G.G.C., L.Z.L., and M.Y.L.; writing, review and/or revision of the manuscript: L.Z.L. and M.Y.L. All the authors have read the authorship agreement of the journal and that the manuscript has been reviewed by and approved by all named authors.

DECLARATION OF INTERESTS

The authors have no conflict of interests to declare.

Received: June 13, 2023
Revised: July 14, 2023
Accepted: July 21, 2023
Published: July 27, 2023

REFERENCES

1. Bray, F., Ferlay, J., Soerjomataram, I., Siegel, R.L., Torre, L.A., and Jemal, A. (2018). Global cancer statistics 2018: GLOBOCAN estimates of incidence and mortality worldwide for 36 cancers in 185 countries. CA. Cancer J. Clin. *68*, 394–424. https://doi.org/10.3322/caac.21492.

2. Li, M.Y., Liu, L.Z., and Dong, M. (2021). Progress on pivotal role and application of exosome in lung cancer carcinogenesis, diagnosis, therapy and prognosis. Mol. Cancer *20*, 22. https://doi.org/10.1186/s12943-021-01312-y.

3. Arbour, K.C., and Riely, G.J. (2019). Systemic Therapy for Locally Advanced and Metastatic Non-Small Cell Lung Cancer: A Review. JAMA *322*, 764–774. https://doi.org/10.1001/jama.2019.11058.

4. Pirker, R. (2020). Conquering lung cancer: current status and prospects for the future. Pulmonology *26*, 283–290. https://doi.org/10.1016/j.pulmoe.2020.02.005.

5. Stepanov, I., Upadhyaya, P., Carmella, S.G., Feuer, R., Jensen, J., Hatsukami, D.K., and Hecht, S.S. (2008). Extensive metabolic activation of the tobacco-specific carcinogen 4-(methylnitrosamino)-1-(3-pyridyl)-1-butanone in smokers. Cancer Epidemiol. Biomarkers Prev. *17*, 1764–1773.

6. Schuller, H.M. (2009). Is cancer triggered by altered signalling of nicotinic acetylcholine receptors? Nat. Rev. Cancer *9*, 195–205. https://doi.org/10.1038/nrc2590.

7. Wu, C.H., Lee, C.H., and Ho, Y.S. (2011). Nicotinic acetylcholine receptor-based blockade: applications of molecular targets for cancer therapy. Clin. Cancer Res. *17*, 3533–3541. https://doi.org/10.1158/1078-0432.CCR-10-2434.

8. Lam, D.C.L., Girard, L., Ramirez, R., Chau, W.S., Suen, W.S., Sheridan, S., Tin, V.P.C., Chung, L.P., Wong, M.P., Shay, J.W., et al. (2007). Expression of nicotinic acetylcholine receptor subunit genes in non-small-cell lung cancer reveals differences between smokers and nonsmokers. Cancer Res. *67*, 4638–4647. https://doi.org/10.1158/0008-5472.CAN-06-4628.

9. Li, Q., Zhou, X., Kolosov, V.P., and Perelman, J.M. (2012). The expression and pharmacological characterization of nicotinic acetylcholine receptor subunits in HBE16 airway epithelial cells. Cell Biochem. Biophys. *62*, 421–431. https://doi.org/10.1007/s12013-011-9324-z.

10. Improgo, M.R., Soll, L.G., Tapper, A.R., and Gardner, P.D. (2013). Nicotinic acetylcholine receptors mediate lung cancer growth. Front. Physiol. *4*, 251. https://doi.org/10.3389/fphys.2013.00251.

11. Pepino, M.Y., Kuda, O., Samovski, D., and Abumrad, N.A. (2014). Structure-function of CD36 and importance of fatty acid signal transduction in fat metabolism. Annu. Rev. Nutr. *34*, 281–303. https://doi.org/10.1146/annurev-nutr-071812-161220.

12. Glatz, J.F.C., Luiken, J.J.F.P., and Bonen, A. (2010). Membrane fatty acid transporters as regulators of lipid metabolism: implications for metabolic disease. Physiol. Rev. *90*, 367–417. https://doi.org/10.1152/physrev.00003.2009.

13. Huang, M.M., Bolen, J.B., Barnwell, J.W., Shattil, S.J., and Brugge, J.S. (1991). Membrane glycoprotein IV (CD36) is physically associated with the Fyn, Lyn, and Yes protein-tyrosine kinases in human platelets. Proc Natl Acad Sci USA *88*, 7844–7848.

14. Zhu, B., Li, M.Y., Lin, Q., Liang, Z., Xin, Q., Wang, M., He, Z., Wang, X., Wu, X., Chen, G.G., et al. (2020). Lipid oversupply induces CD36 sarcolemmal translocation via dual modulation of PKCzeta and TBC1D1: an early event prior to insulin resistance. Theranostics *10*, 1332–1354. https://doi.org/10.7150/thno.40021.

15. Pascual, G., Avgustinova, A., Mejetta, S., Martín, M., Castellanos, A., Attolini, C.S.O., Berenguer, A., Prats, N., Toll, A., Hueto, J.A., et al. (2017). Targeting metastasis-initiating cells through the fatty acid receptor CD36. Nature *541*, 41–45. https://doi.org/10.1038/nature20791.

16. Nath, A., and Chan, C. (2016). Genetic alterations in fatty acid transport and metabolism genes are associated with metastatic progression and poor prognosis of human cancers. Sci. Rep. *6*, 18669. https://doi.org/10.1038/srep18669.

17. Hale, J.S., Otvos, B., Sinyuk, M., Alvarado, A.G., Hitomi, M., Stoltz, K., Wu, Q., Flavahan, W., Levison, B., Johansen, M.L., et al. (2014). Cancer stem cell-specific scavenger receptor CD36 drives glioblastoma progression. Stem Cell. *32*, 1746–1758. https://doi.org/10.1002/stem.1716.

18. Nath, A., Li, I., Roberts, L.R., and Chan, C. (2015). Elevated free fatty acid uptake via CD36 promotes epithelial-mesenchymal transition in hepatocellular carcinoma. Sci. Rep. *5*, 14752. https://doi.org/10.1038/srep14752.

19. Yeatman, T.J. (2004). A renaissance for SRC. Nat. Rev. Cancer *4*, 470–480. https://doi.org/10.1038/nrc1366.

20. Giaccone, G., and Zucali, P.A. (2008). Src as a potential therapeutic target in non-small-cell lung cancer. Ann. Oncol. *19*, 1219–1223. https://doi.org/10.1093/annonc/mdn048.

21. Shen, J., Xu, L., Owonikoko, T.K., Sun, S.Y., Khuri, F.R., Curran, W.J., and Deng, X. (2012). NNK promotes migration and invasion of lung cancer cells through activation of c-Src/PKCiota/FAK loop. Cancer Lett. *318*, 106–113. https://doi.org/10.1016/j.canlet.2011.12.008.

22. Qin, B., Ariyama, H., Baba, E., Tanaka, R., Kusaba, H., Harada, M., and Nakano, S. (2006). Activated Src and Ras induce gefitinib resistance by activation of signaling pathways downstream of epidermal growth factor receptor in human gallbladder adenocarcinoma cells. Cancer Chemother. Pharmacol. *58*, 577–584. https://doi.org/10.1007/s00280-006-0219-4.

23. Lan, T., Wang, H., Zhang, Z., Zhang, M., Qu, Y., Zhao, Z., Fan, X., Zhan, Q., Song, Y., and Yu, C. (2017). Downregulation of beta-arrestin 1 suppresses glioblastoma cell malignant progression vis inhibition of Src signaling. Exp. Cell Res. *357*, 51–58. https://doi.org/10.1016/j.yexcr.2017.04.023.

24. MacAuley, A., and Cooper, J.A. (1989). Structural differences between repressed and derepressed forms of p60c-src. Mol. Cell Biol. *9*, 2648–2656. https://doi.org/10.1128/mcb.9.6.2648-2656.1989.

25. Li, M.Y., Liu, L.Z., Li, W., Ng, C.S.H., Liu, Y., Kong, A.W.Y., Zhao, Z., Wang, S., Qi, H., Jia, H., et al. (2019). Ambient fine particulate matter inhibits 15-lipoxygenases to promote lung carcinogenesis. J. Exp. Clin. Cancer Res. *38*, 359. https://doi.org/10.1186/s13046-019-1380-z.

26. Li, M.Y., Yuan, H., Ma, L.T., Kong, A.W.Y., Hsin, M.K.Y., Yip, J.H.Y., Underwood, M.J., and Chen, G.G. (2010). Roles of peroxisome proliferator-activated receptor-alpha and -gamma in the development of non-small cell lung cancer. Am. J. Respir. Cell Mol. Biol. *43*, 674–683. https://doi.org/10.1165/rcmb.2009-0349OC.

27. Schuller, H.M. (2002). Mechanisms of smoking-related lung and pancreatic adenocarcinoma development. Nat. Rev. Cancer *2*, 455–463. https://doi.org/10.1038/nrc824.

28. Brunnemann, K.D., Mitacek, E.J., Liu, Y., Limsila, T., and Suttajit, M. (1996). Assessment of major carcinogenic tobacco-specific N-nitrosamines in Thai cigarettes. Cancer Detect. Prev. *20*, 114–121.

29. Proulx, L.I., Gaudreault, M., Turmel, V., Augusto, L.A., Castonguay, A., and Bissonnette, E.Y. (2005). 4-(Methylnitrosamino)-1-(3-pyridyl)-1-butanone, a component of tobacco smoke, modulates mediator release from human bronchial and alveolar epithelial cells. Clin. Exp. Immunol. *140*, 46–53. https://doi.org/10.1111/j.1365-2249.2005.02739.x.

30. Proulx, L.I., Paré, G., and Bissonnette, E.Y. (2007). Alveolar macrophage cytotoxic activity is inhibited by 4-(methylnitrosamino)-1-(3-pyridyl)-1-butanone (NNK), a carcinogenic component of cigarette smoke. Cancer Immunol. Immunother. *56*, 831–838. https://doi.org/10.1007/s00262-006-0243-6.

31. Li, M.Y., Yip, J., Hsin, M.K.Y., Mok, T.S.K., Wu, Y., Underwood, M.J., and Chen, G.G. (2008). Haem oxygenase-1 plays a central role in NNK-mediated lung carcinogenesis. Eur. Respir. J. *32*, 911–923.

32. Khandekar, M.J., Cohen, P., and Spiegelman, B.M. (2011). Molecular mechanisms of cancer development in obesity. Nat. Rev. Cancer *11*, 886–895. https://doi.org/10.1038/nrc3174.

33. Ye, H., Adane, B., Khan, N., Sullivan, T., Minhajuddin, M., Gasparetto, M., Stevens, B., Pei, S., Balys, M., Ashton, J.M., et al. (2016). Leukemic Stem Cells Evade Chemotherapy by Metabolic Adaptation to an Adipose Tissue Niche. Cell Stem Cell *19*, 23–37. https://doi.org/10.1016/j.stem.2016.06.001.

34. Chen, Y.J., Liao, W.X., Huang, S.Z., Yu, Y.F., Wen, J.Y., Chen, J., Lin, D.G., Wu, X.Y., Jiang, N., and Li, X. (2021). Prognostic and immunological role of CD36: A pan-cancer analysis. J. Cancer *12*, 4762–4773. https://doi.org/10.7150/jca.50502.

35. Liu, L.Z., Wang, M., Xin, Q., Wang, B., Chen, G.G., and Li, M.Y. (2020). The permissive role of TCTP in PM2.5/NNK-induced epithelial-mesenchymal transition in lung cells. J. Transl. Med. *18*, 66. https://doi.org/10.1186/s12967-020-02256-5.

36. Yang, P., Su, C., Luo, X., Zeng, H., Zhao, L., Wei, L., Zhang, X., Varghese, Z., Moorhead, J.F., Chen, Y., and Ruan, X.Z. (2018). Dietary oleic acid-induced CD36 promotes cervical cancer cell growth and metastasis via up-regulation Src/ERK pathway. Cancer Lett. *438*, 76–85. https://doi.org/10.1016/j.canlet.2018.09.006.

37. Canton, J., Neculai, D., and Grinstein, S. (2013). Scavenger receptors in homeostasis and immunity. Nat. Rev. Immunol. *13*, 621–634. https://doi.org/10.1038/nri3515.

38. Glatz, J.F.C., Luiken, J.J.F.P., and Bonen, A. (2010). Membrane fatty acid transporters as regulators of lipid metabolism: implications for metabolic disease. Physiol. Rev. *90*, 367–417.

39. Li, Z., and Kang, Y. (2017). Lipid Metabolism Fuels Cancer's Spread. Cell Metab. *25*, 228–230. https://doi.org/10.1016/j.cmet.2017.01.016.

40. Cha, J.Y., and Lee, H.J. (2016). Targeting Lipid Metabolic Reprogramming as Anticancer Therapeutics. J. Cancer Prev. *21*, 209–215. https://doi.org/10.15430/JCP.2016.21.4.209.

41. Bonelli, M., Terenziani, R., Zoppi, S., Fumarola, C., La Monica, S., Cretella, D., Alfieri, R., Cavazzoni, A., Digiacomo, G., Galetti, M., and Petronini, P.G. (2020). Dual Inhibition of CDK4/6 and PI3K/AKT/mTOR Signaling Impairs Energy Metabolism in MPM Cancer Cells. Int. J. Mol. Sci. *21*, 5165. https://doi.org/10.3390/ijms21145165.

42. Luo, X., Zheng, E., Wei, L., Zeng, H., Qin, H., Zhang, X., Liao, M., Chen, L., Zhao, L., Ruan, X.Z., et al. (2021). The fatty acid receptor CD36 promotes HCC progression through activating Src/PI3K/AKT axis-dependent aerobic glycolysis. Cell Death Dis. *12*, 328. https://doi.org/10.1038/s41419-021-03596-w.

43. Bjorge, J.D., Jakymiw, A., and Fujita, D.J. (2000). Selected glimpses into the activation and function of Src kinase. Oncogene *19*, 5620–5635. https://doi.org/10.1038/sj.onc.1203923.

44. Mazurenko, N.N., Kogan, E.A., Zborovskaya, I.B., and Kisseljov, F.L. (1992). Expression of pp60c-src in human small cell and non-small cell lung carcinomas. Eur. J. Cancer *28*, 372–377. https://doi.org/10.1016/s0959-8049(05)80056-5.

45. Budde, R.J., Ke, S., and Levin, V.A. (1994). Activity of pp60c-src in 60 different cell lines derived from human tumors. Cancer Biochem. Biophys. *14*, 171–175.

46. Dasgupta, P., Rastogi, S., Pillai, S., Ordonez-Ercan, D., Morris, M., Haura, E., and Chellappan, S. (2006). Nicotine induces cell proliferation by beta-arrestin-mediated activation of Src and Rb-Raf-1 pathways. J. Clin. Invest. *116*, 2208–2217. https://doi.org/10.1172/JCI28164.

47. Pillai, S., Trevino, J., Rawal, B., Singh, S., Kovacs, M., Li, X., Schell, M., Haura, E., Bepler, G., and Chellappan, S. (2015). -Arrestin-1 Mediates Nicotine-Induced Metastasis through E2F1 Target Genes That Modulate Epithelial-Mesenchymal Transition. Cancer Res. *75*, 1009–1020. https://doi.org/10.1158/0008-5472.can-14-0681.

48. Song, L., Morris, M., Bagui, T., Lee, F.Y., Jove, R., and Haura, E.B. (2006). Dasatinib (BMS-354825) selectively induces apoptosis in lung cancer cells dependent on epidermal growth factor receptor signaling for survival. Cancer Res. *66*, 5542–5548. https://doi.org/10.1158/0008-5472.CAN-05-4620.

49. Elisia, I., Cho, B., Hay, M., Li, M.Y., Hofs, E., Lam, V., Dyer, R.A., Lum, J., and Krystal, G. (2019). The effect of diet and exercise on tobacco carcinogen-induced lung cancer. Carcinogenesis *40*, 448–460. https://doi.org/10.1093/carcin/bgz060.

50. Saad, M.I., McLeod, L., Yu, L., Ebi, H., Ruwanpura, S., Sagi, I., Rose-John, S., and Jenkins, B.J. (2020). The ADAM17 protease promotes tobacco smoke carcinogen-induced lung tumorigenesis. Carcinogenesis *41*, 527–538. https://doi.org/10.1093/carcin/bgz123.

51. Weller, P., Bankfalvi, A., Gu, X., Dominas, N., Lehnerdt, G.F., Zeidler, R., Lang, S., Brandau, S., and Dumitru, C.A. (2014). The role of tumour FoxP3 as prognostic marker in different subtypes of head and neck cancer. Eur. J. Cancer *50*, 1291–1300. https://doi.org/10.1016/j.ejca.2014.02.016.

STAR★METHODS

KEY RESOURCES TABLE

REAGENT or RESOURCE	SOURCE	IDENTIFIER
Antibodies		
Recombinant Anti-CD36 antibody	Abcam	Cat# ab133625; RRID:AB_2716564
Anti-CD36 antibody	Abcam	Cat# ab23680; RRID:AB_447608
Anti-Nicotinic Acetylcholine Receptor alpha 7 antibody	Abcam	Cat# ab216485
Anti-Src antibody	Abcam	Cat# ab16885; RRID:AB_443522
Recombinant Anti-Sodium Potassium ATPase antibody	Abcam	Cat# ab76020; RRID:AB_1310695
Phospho-Src Family (Tyr416) (D49G4) Rabbit mAb	Cell Signaling Technology	Cat# 6943S; RRID:AB_10013641
Phospho-Src (Tyr527) Antibody	Cell Signaling Technology	Cat# 2105S; RRID:AB_331034
Phospho-Akt (Ser473) Antibody	Cell Signaling Technology	Cat# 9271S; RRID:AB_329825
Phospho-Akt (Thr308) Antibody	Cell Signaling Technology	Cat# 9275S; RRID:AB_329828
Akt Antibody	Cell Signaling Technology	Cat# 9272S; RRID:AB_329827
Phospho-p44/42 MAPK (Erk1/2) (Thr202/Tyr204) Rabbit mAb	Cell Signaling Technology	Cat# 4370S; RRID:AB_2315112
p44/42 MAPK (Erk1/2) (137F5) Rabbit mAb	Cell Signaling Technology	Cat# 4695S; RRID:AB_390779
GAPDH (D16H11) Rabbit mAb	Cell Signaling Technology	Cat# 5174S; RRID:AB_10622025
Anti-mouse IgG, HRP-linked Antibody	Cell Signaling Technology	Cat# 7076; RRID:AB_330924
Anti-rabbit IgG, HRP-linked Antibody	Cell Signaling Technology	Cat# 7074; RRID:AB_2099233
Goat anti-Rabbit IgG (H+L) Highly Cross-Adsorbed Secondary Antibody	ThermoFisher	Cat# A11035
Goat anti-Mouse IgG (H+L) Cross-Adsorbed Secondary Antibody	ThermoFisher	Cat# A11003
Goat anti-Rabbit IgG (H+L) Highly Cross-Adsorbed Secondary Antibody	ThermoFisher	Cat# A11034
Goat anti-Mouse IgG (H+L) Cross-Adsorbed Secondary Antibody	ThermoFisher	Cat# A11001
CD36 Antibody	Santa Cruz	Cat# sc-7309; RRID:AB_627044
Src Antibody	Santa Cruz	Cat# sc-5266; RRID:AB_627308
Bacterial and virus strains		
Subcloning Efficiency DH5a	ThermoFisher	Cat# 18265017
Lentivirus	WZ Biosciences Inc	N/A
Biological samples		
Lung cancer patients tissue sections; See Table S1	Prince of Wales Hospital	N/A
A/J mice lung tissue sections	This paper	N/A
Nude mice subcutaneous tumors	This paper	N/A
Chemicals, peptides, and recombinant proteins		
4-(Methylnitrosamino)-1-(3-pyridyl)-1-butanone (NNK)	Chemsyn Science Laboratories	Cat# M325750
Benzethonium Chloride	Selleck	Cat# S4162

(*Continued on next page*)

Continued

REAGENT or RESOURCE	SOURCE	IDENTIFIER
Methyllycaconitine citrate	Med Chem Express	Cat# HY-N2332A
Dasatinib	Med Chem Express	Cat# HY-10181
SU6656	Sigma	Cat# S9692
Sulfosuccinimidyl Oleate	Cayman Chemical	Cat# 11211
Mitomycin-C	Sigma	Cat# 47589-M
Critical commercial assays		
VECTASTAIN® ABC-HRP Kit, Peroxidase (Standard)	Vector Laboratories	Cat# PK-4000
PrimeScript™ RT reagent Kit	Takara	Cat# RR037A
MTS Kit	Promega	Cat# G3580
ECL detection reagent	Pierce	Cat# PI32106
Bicinchoninic Acid Kit for Protein Determination	Sigma	Cat# BCA1
Experimental models: Cell lines		
NCI-H23	ATCC	Cat# CRL-5800
A549	ATCC	Cat# CCL-185
Bet1A	Gift of J. E. Lechner, Laboratory of Human Carcinogenesis, National Cancer Institute	N/A
Experimental models: Organisms/strains		
Nude mice	GemPharmatech	Cat# D000521
Wild type C57 BL/6J mice	GemPharmatech	Cat# N000295
Wild type A/J mice	GemPharmatech	Cat# N000018
$CD36^{-/+}$ C57 BL/6J mice	GemPharmatech	Cat# T010474
$CD36^{-/-}$ A/J mice	This paper	N/A
Oligonucleotides		
CD36 shRNA: 5′-GGACCATTGGTGATGAGAAGG CAAACATG-3′	Origene	Cat# TL314090
Primers for A/J mice genetic background detection, See Table S3	This paper	N/A
Primers for examination of nAChR subtypes in lung cells, See Figure S1D	This paper	N/A
Primers for C57 BL/6J and A/J mice genotyping, See Figure S8A	This paper	N/A
Recombinant DNA		
pLent-U6-GFP-Puro-CD36 shRNAs	Origene	Cat# TL314090
Software and algorithms		
GraphPad Prism 8	GraphPad	https://www.graphpad.com/scientificsoftware/prism/
Image J	NIH	https://ImageJ.nih.gov/ij/
Kaplan-Meier Plotter	Kaplan-meier Plotter Database	http://kmplot.com/analysis/

RESOURCE AVAILABILITY

Lead contact

Further information and requests for resources and reagents should be directed to and will be fulfilled by the lead contact, Li-Zhong Liu (liulz@szu.edu.cn).

Materials availability

This Study did not generate new unique reagents.

Data and code availability

- All data reported in this paper will be shared by the lead contact upon request.
- This paper does not report original code.
- Any additional information required to reanalyze the data reported in this paper is available from the lead contact upon request.

EXPERIMENTAL MODEL AND SUBJECT DETAILS

LUAD cancer sample collection

65-Paired human primary LUAD and adjacent normal lung tissues were collected immediately after surgical resection at the Prince of Wales Hospital (Hong Kong, China). The study was performed in accordance with the ethical principles and guidelines for human research of the Helsinki Declaration, and human ethics approval (2014.649 and 2015.729) was obtained from the joint Chinese University of Hong Kong-New Territories East Cluster Clinical Research Governance and Management Committee. An informed consent for human tissues for research purposes only was obtained from all patients recruited. Tumor tissue samples were taken from the central part of the tumors. Of the 65 patients, 14 were current cigarette smokers with an average smoking history of 35 years, 20 patients were previous cigarette smokers with an average smoking history of 28 years, and the other 31 patients were non-smokers. For patient sample details, please refer to Table S1. All tumor and non-tumor tissue specimens were confirmed by histological examination. The specimens were snap-frozen in liquid nitrogen and stored at -80°C and were also fixed in 10% formalin and embedded for histochemical staining examination.

Animal treatment

The experimental protocol, and care and handling of the animals were approved by the Animal Research Ethical Committee of Shenzhen University. Female/male strain A/J mice were purchased from GemPharmatech Co., Ltd, Jiangsu, China. Female A/J mice are more prone than their male counterparts to NNK-induced lung nodules.[49] For investigation of CD36 expression in LUAD development, female A/J mice at 6 weeks of age were randomly injected intraperitoneally (*i.p*) three times on alternate days with either NNK (100 mg/kg in 0.3 ml PBS, Chemsyn Science Laboratories , Lenexa, KS), or equivalent volume of physiological saline as a control. Starting at 14 weeks after NNK treatment, 9 mice in each group were killed every one week. The killing lasted until Week 16.

To investigate the role of CD36 in NNK-induced LUAD development, CD36 knockout (KO) A/J mice model were constructed. First, $CD36^{+/-}$ mice with C57BL/6J background were produced by GemPharmatech Co., Ltd, Jiangsu, China. Then $CD36^{+/-}$ C57BL/6J were back-crossed with WT A/J mice for five generations to produce mice with A/J background, which were susceptible to the carcinogenic effects of NNK.[49,50] Homologous knockout of CD36 ($CD36^{-/-}$) were confirmed by genotyping. KO ($CD36^{-/-}$) and WT (wild type, $CD36^{+/+}$) A/J mice (female, 6 weeks old) were randomly placed into the experimental or control groups. A/J mice were injected intraperitoneally (*i.p*) three times on alternate days with either NNK (100 mg/kg in 0.3 ml PBS, Chemsyn Science Laboratories, Lenexa, KS), or equivalent volume of physiological saline as a control. Five mice in each group were humanely culled 16 weeks later. Lungs were collected for further analysis.

Cell culture

Lung cancer cell lines NCI-H23 (CRL-5800) and A549 (CCL-185) were purchased from ATCC (www.atcc.org). Lung normal bronchial epithelial cells Bet1A described in our previous study[25] was used. Bet1A was cultured in medium LHC-9, and NCI-H23 and A549 cells were cultured in DMEM supplemented with 10% inactivated FBS (Invitrogen, Carlsbad, CA).

Transient transfection and establishment of stable cell lines

The Lentivirus vectors of three CD36 shRNAs termed as pLent-U6-GFP-Puro-CD36 shRNAs, and one scramble shRNA termed as pLent-U6-GFP-Puro-Scramble shRNA were obtained from Origene (Rockville, MD). The shRNAs were transfected into the cells with X-treme GENE HP DNA Transfection Reagent (Roche,

St. Louis, MO) according to the kit instruction. Cells were maintained for another 48h to express the exogenous genes. After testing, the selected CD36 shRNA sequence given the best inhibition effect was 5′-GGACCATTGGTGATGAGAAGGCAAACATG-3′. Then the plasmids (pLent-U6-GFP-Puro) containing the selected CD36 shRNA and scramble-shRNA were packed into lentivirus respectively by Weizhen Biotechnology Co., Ltd (Shandong, China). The virus particles were used to infect cells and then selected by 1 μg/mL puromycin (Sigma-Aldrich, MO) for 3 days to produce stable transfected cells (designated as NCI-H23-ShCD36, Bet1A-ShCD36, A549-ShCD36, NCI-H23-Scramble, Bet1A-Scramble, and A549-Scramble, respectively). Knockdown efficiency was confirmed at protein levels.

Xenograft model

All animal experiments were conducted in accordance with the Animals (Control of Experiments) Ordinance Chapter 340, and approved by the Animal Experimentation Ethics Committee of Shenzhen University. Our previous study proved that lung cells treated by 10 μM NNK for a longer period of 28 days exhibited significantly higher proliferation property and maintain an epithelial mesenchymal transition state than the non-treated control cells.[25] The nude mice were transplanted subcutaneously with constructed LUAD cells treated with or without NNK for 28 days (designated as NCI-H23-ShCD36, NCI-H23-ShCD36-NNK, NCI-H23-Scramble, NCI-H23-Scramble-NNK, A549-ShCD36, A549-ShCD36-NNK, A549-Scramble, and A549-Scramble-NNK, respectively) for tumorigenicity assay. Briefly, the designated cells ($1x10^6$) were S.C. implanted into the left and right dorsal flank of 4-week-old male nude mice (nu/nu, n=10/group, randomized group), respectively. Tumors were measured in two dimensions by external caliper and Tumor volume (V) was estimated by formula [length x width $(mm)^2$]/2.[25] The size of tumor was monitored for 6 weeks. At the endpoint, the mice were sacrificed by cervical dislocation while under using overdose of sodium pentobarbital and tumors were harvested and measured. For lung metastasis formation, $5x10^5$ A549-shCD36, A549-shCD36-NNK, A549-scramble and A549-scramble-NNK cells were injected into the lateral tail vein of the nude mice respectively. Mice were euthanized 12 weeks after injection, and the lung, liver and spleen of each mouse were subjected to formaldehyde fixation and followed by H&E and IHC staining. For CD36 irreversible inhibitor SSO influence on LUAD cell lung metastasis formation, $5x10^5$ A549, A549-NNK, A549-SSO and A549-NNK-SSO cells were injected into the lateral tail vein of the nude mice respectively. Mice were killed 12 weeks after injection, and the lung, liver and spleen of each mouse were subjected to formaldehyde fixation and followed by H&E and IHC staining.

METHODS DETAILS

The OS (overall survival) analysis by Kaplan–Meier plotter software

Based on online survival analysis software: Kaplan–Meier Plotter (http://kmplot.com/analysis/), the OS of the two groups of patients (n=820) with high and low CD36 expression in NSCLC tissues were calculated.

Western-blot

Western-blot was performed as our previous description.[14] Aliquots proteins were separated by SDS-PAGE (10% polyacrylamide). Thereafter, proteins were electrophoretically transferred to polyvinylidene difluoride membrane and blocked in 5% BSA and 0.05% Tween 20 in Tris-buffered saline (TBST) for 1 h at room temperature. Membranes were incubated overnight at 4°C with the indicated first antibodies. Membranes were washed (3 times for 5 min each) in TBST and incubated with horseradish peroxidase-conjugated IgG for 1 h at room temperature, followed by additional washes (3 times for 15 min) in TBST. Proteins were visualized by ECL and quantified by densitometric scanning with Image J and analyzed with GraphPad Prism software, and the result was presented by the relative intensity of control condition based on GAPDH normalization for total protein. Antibodies of CD36 (ab133625, ab23680), α7nAChR (ab216485), Src (ab16885) were purchased from Abcam (Cambridge, MA). p-Src-Tyr416 (6943S), p-Src-Tyr527 (2105S), p-Akt473 (9271s), p-Akt308 (9275S), Akt (9272S), p-ERK1/2 (4370S), ERK1/2 (4695S), GAPDH (5174S) were obtained from Cell Signaling (Boston, MA). The anti-mouse (7076) and anti-rabbit (7074) HRP-linked anti-IgGs were purchased from Cell Signaling (Boston, MA).

Immunohistochemistry (IHC), immunofluorescence (IF) and haematoxylin-eosin (H&E) staining

The tissues in formalin-fixed paraffin sections were sliced into 5μm thickness. For cells, after proper treatments, cells were fixed with 3% paraformaldehyde in PBS. IHC was performed according to the procedure of ABC-HRP kit (Vector Laboratories, Burlinegame, CA) and protein expression levels were scored 1 to 12

according to the IRS method.[35,51] The immunoreactive score (IRS) was calculated as intensity of the staining reaction multiplied by the percentage of positive cells. IF was performed as described previously.[25] Both tissue and cell samples were washed with 0.1 mol/l glycine in PBS for 10 min and permeabilized with 0.1% (vol/vol) Triton X-100 in PBS for 3 min, and then blocked with 5% BSA. After washing with PBS, the samples were incubated with primary antibodies and subsequently incubated with either Alexa-conjugated goat anti-rabbit or anti-mouse secondary antibodies respectively. Samples were mounted in ProLong Antifade solution containing DAPI onto glass slides. H&E staining was performed using 5μm paraffin sections of the tissues stained with haematoxylin-eosin for 5 min. Antibodies of CD36 (ab133625), ATPase (ab76020), α7nAChR (ab216485) and Src (ab16885) were purchased from Abcam (Cambridge, MA). Antibodies of Biotinylated goat anti-rabbit IgGs (Vector Laboratories, Burlinegame, CA), Fluor 546 goat anti-rabbit/anti-mouse (A11035/ A11003), and Fluor 488 goat anti-rabbit/anti-mouse (A11034/A11001) were purchased from Invitrogen (Carlsbad, CA). The stained cells were examined using the Leica microscopy (Aperio CS2, Vista, CA) or the Zeiss Spot imaging system (Carl Zeiss, Jena, Germany).

Quantitative RT-PCR

Total RNA was extracted using Trizol reagent (Invitrogen, Grand Island, NY). cDNA was synthesized using PrimeScript™ RT reagent Kit (Takara, Japan). RT-PCR reactions were conducted using Premix Taq™ (Takara, Japan) and QuantStudio 3 Real-Time PCR Instrument system (ThermoFisher, Waltham, MA). The primer sequences[8] for the targeted regions of nAChR subtypes and 18S were summarized in Figure S1D. RT-PCR reactions consisted of the following steps: 94°C 5 min, 35 cycles at 94°C 30s, 55°C 30s and 72°C 30s.

F5 A/J mice genetic background detection

Genomic DNA was extracted from ear samples of mice. The collected ear tissues were digested with alkaline lysis reagent and neutralized with 40 mM Tris-HCl (pH = 5). Genomic DNA samples were subjected to a PCR assay with primers as reported in Table S3. The PCR reaction condition was 94°C, 5 min, followed by 35 cycles of 94°C, 30 s; 55°C, 30 s; and 72°C, 30 s, then 72°C, 7 min. The amplified PCR products were resolved on 3% agarose gels with 0.5 μg/ml ethidium bromide, visualized and photographed.

Assessment of cell viability

Cell viability was detected by MTT assay using MTS kit (G3580, Progema, Beijing) according to the manufacturer's instructions.

Wound healing and transwell assay

Cells ($5x10^5$ cells/well) under different treatments were seeded in 24-well plates (Corning, New York) and used for wound healing assay.[35] To assess cell motility, cells under different treatments ($5x10^5$ cells/ mL) were seeded in 24-well plates (Corning, New York). Non-treated cells were set up as the control. The cells were incubated with 10 μg/ml mitomycin-C (Sigma, MO) for 2 h and then starved in serum-free medium for 24 h to suppress proliferation. The monolayers of cell were scraped with a sterile 200-μl micropipette tip (0 h) to create a denuded zone with a constant width and were washed twice with phosphate-buffered saline (PBS) to remove cellular debris. The cells were cultured in culture medium without FBS. The scratched monolayers were imaged for 24 h or 48 h using an inverted microscope (Olympus, Japan) in a blinded fashion. The relative percentage of wound healed was analysis by Image J software. For transwell assay, cell migration and invasion were determined using Corning Transwell plate with polycarbonate membrane (*dp*8.0μm) and Transwell plate with BioCoat Matrigel Invasion Chamber (Corning, NY) respectively. Cells (2×10^4 cells/well) under different treatments were seeded and used for transwell assay.[35] Cells under different treatments were incubated with 10 μg/ml mitomycin-C (Sigma, MO) for 2 h and then starved in serum-free medium for 24 h to suppress proliferation. Cells (2×10^4 cells/well) were seeded onto the top chamber in serum-free cell culture medium. Complete culture medium (supplemented with 10% FBS) was added to the bottom chamber as a chemoattractant. After 48 hours, cells that had invaded through the membrane were stained with 0.1% Crystal violet. Migrated cells in randomly selected fields were observed by light microscopy (Olympus, Japan).

Co-immunoprecipitation (Co-IP)

Co-IP were performed as our previous description.[14] Precleared cell lysates were incubated with the indicated antibodies or control IgG under constant rotation at 4°C overnight. Antibodies against CD36 (sc-7309) and Src (sc-5266) were from Santa Cruz (Dallas, TX), and α7nAChR (ab216485) were from Abcam

(Cambridge, MA). Then the protein extracts were incubated with the equilibrated Pierce Protein A/G Plus (ThermoFisher,Waltham, MA) at 4°C for 2 hours with gentle mixing to bind the specific antibody captured proteins. Immunoprecipitates captured with protein A/G-agarose were washed 3 times with the lysis buffer. Beads were finally collected and the bounded fusion proteins were eluted from the beads for further western blot analysis.

QUANTIFICATION AND STATISTICAL ANALYSIS

Statistical analyses were performed using GraphPad Prism, version 8.0 (GraphPad Software). To compare the difference between two groups, independent sample t test, paired t-test, or Mann–Whitney U test was used. The clinic-pathologic features in patients with relative expressing CD36 were compared using Pearson's chi-squared test, basing on the CD36 expression levels in tumor tissue was graded as normal/high expression in comparison with the non-tumor tissue. Kaplan-Meier plots and log-rank test were used for survival analysis. $p<0.05$ was considered statistically significant.